Available online at www.sciencedirect.com
SCIENCE DIRECT®
Coordination Chemistry Reviews 248 (2004) 1025–1045
COORDINATION CHEMISTRY REVIEWS
www.elsevier.com/locate/ccr

Recent developments in the synthesis and properties of diruthenium tetracarboxylates

Manuel A.S. Aquino*

Department of Chemistry, St. Francis Xavier University, P.O. Box 5000, Antigonish, NS, Canada B2G 2W5

Received 11 February 2004; accepted 24 June 2004

Contents

Abstract

The chemistry of diruthenium tetracarboxylates has grown substantially since our initial review in 1998. This update of the literature through 2003 covers the versatile synthetic aspects of the $[Ru_2(\mu\text{-}O_2CR)_4L_n]^{m+}$ (n = 1 or 2, m = 0–2) "building block", for both mixed-valent Ru_2(II,III) and reduced Ru_2(II,II) cores, in which R can include a wide variety of alkyl, alkoxy, aryl, or metallocenyl groups (including chiral groups) with the axial L group normally being a neutral Lewis base or a halide but could also be a weakly coordinating counterion such as ClO_4^- or BF_4^-. The $[Ru_2(\mu\text{-}O_2CR)_4L_n]^{m+}$ unit has been linked together, through the judicious choice of axial or equatorial bridging ligands, into a variety of polymeric or network structures that display interesting magnetic, electronic, mesomorphic, occlusion and catalytic properties. The use of biologically relevant and/or hydrophilic R and L groups has also lead to the study of anti-tumor and anti-inflammatory properties.

Keywords: Diruthenium tetracarboxylates; Magnetism; Mesogens; Polymers; Anticancer

* Corresponding author. Tel.: +1 902 867 5336; fax: +1 902 867 2414.
E-mail address: maquino@stfx.ca.

0010-8545/$ – see front matter © 2004 Elsevier B.V. All rights reserved.
doi:10.1016/j.ccr.2004.06.016

1. Introduction

In the 6 years since the appearance of our previous review [1], on the aspects of diruthenium (and diosmium) tetracarboxylates, a wealth of new work by various groups has exploited the versatility of these compounds. Two reviews, one covering the career of Giroud-Godquin and her research in the field of metallomesogens [2] and a general review on ruthenium-acetato complexes [3], appeared in 1998 and 1999, respectively. These deal with very limited aspects of diruthenium tetracarboxylate chemistry with most of the material already covered to a great extent in our earlier paper.

The primary areas of interest in recent years have been the synthetic modification of the $[Ru_2(\mu\text{-}O_2CR)_4L_2]^{0/+/2+}$ core by varying R and/or L (where R is an alkyl, aryl, metallocenyl group, etc., and L is usually a Lewis base) to form a "building block" with certain desired structural and physical properties and the extension of these building blocks to the construction of larger assemblies, networks, and chains. Once the synthetic hurdles were overcome many of the resulting compounds have been investigated in terms of their magnetic, mesomorphic, catalytic and cytotoxic properties. The magnetic properties have been of particular interest because of the unusually high magnetic moment (∼4.2 B.M., three unpaired electrons) seen in the mixed-valent (Ru_2(II,III)) species due to its unusual electronic configuration, $\sigma^2\pi^4\delta^2(\pi^*\delta^*)^3$, in which the three electrons are spread over the essentially degenerate π^* and δ^* orbitals. Exploitation of this interesting property to generate novel magnetic materials has been the subject of many recent studies.

We shall deal with those studies that focus primarily on the design of novel axial or equatorial adducts (including larger arrays) first, followed by those in which one or more of the above mentioned physical properties have been investigated.

2. Novel axial adducts

Three major aspects of axial coordination to the diruthenium core have been investigated: (1) the effect of varying the donor strength of L on the structural and physical properties of the core, (2) the binding of "biologically relevant" ligands and (3) the binding of very weakly coordinating ligands.

2.1. Varying the donor strength of L

A series of adducts of the form $[Ru_2(\mu\text{-}O_2CCH_3)_4L_2](PF_6)$ were studied with L = various O-donor (urea and its derivatives) [4] and N-donor ligands (pyridine and its derivatives) [5] along with the first examples of structurally characterized S-donor (tetrahydrothiophene, tetramethylthiourea) [4,6] and P-donor (tricyclohexylphosphine) [7] complexes. Taken together with earlier results on the dimethylsulfoxide (dmso), *N*,*N*′-dimethylformamide (dmf) and water adducts [8], Table 1 summarizes the effect these donors have on the Ru–Ru bond length and the redox potential of the $Ru_2^{5+/4+}$ couple.

Table 1
Electrochemical and crystallographic data for various $[Ru_2(\mu\text{-}O_2CCH_3)_4L_2]^+$ adducts

L[a]	$E_{1/2}$ (mV)[b]	M–M (Å)[c]	DN[d]
PCy_3	−730	2.427(1)	–
quin	−671	2.2917(6)	61[e]
tmtu	−541	2.301(2)	–
4-Mepy	−537	2.279(1)	35.1
4-Phpy	−529	2.279(7)	>33.1
py	−519	2.281(5)	33.1
tmu	−487	2.2750(8)	31.0
dmso	−483	2.268(1)	29.8
4-CNpy	−396	2.2741(7)	<33.1
tht	−322	2.285(4)	–
dmf	−302	2.265(1)	26.6
"unligated"[f]	−233	–	1[g]

[a] Cy: cyclohexyl, quin: quinuclidine, tmtu: 1,1,3,3-tetramethyl-2-thiourea, py: pyridine, tmu: 1,1,3,3-tetramethylurea, dmso: dimethylsulfoxide, tht: tetrahydrothiophene, dmf: *N*,*N*′-dimethylformamide.

[b] In 1,2-dichloroethane versus Fc/Fc^+ couple at 25 °C.

[c] S.D. values in brackets.

[d] Gutmann donor number.

[e] Value for triethylamine.

[f] For the $[Ru_2(\mu\text{-octanoate})_4]^{+/0}$ couple in dichloromethane [9] where there are, presumably, still weak $O_{(neighbour\text{-}carboxylate)}$–Ru interactions and it is not truly unligated.

[g] Value for dichloromethane.

As the donor strength increases (reflected for some of the entries by their Gutmann donor numbers) the Ru–Ru bond length increases, presumably due to the increased population of the dimetal-centered antibonding orbitals. This increase is quite small for the O, N and S donors listed but quite large when going from the strongest N-donor (quinuclidine) to PCy_3. The P-donor adduct has the longest Ru–Ru bond, 2.427 Å, of any $[Ru_2(\mu\text{-}O_2CR)_4L_2]^+$ adduct to date (Fig. 1).

The redox potentials ($E_{1/2}$) decrease steadily as the ligand donor strength increases (the increased electron population at the dimetal centers makes them more difficult to reduce) from −233 mV for an "unligated" (which is not truly unligated as there would be weak $O_{(neighbour\text{-}carboxylate)}$–Ru interactions) species [9] to −730 mV for the PCy_3 adduct, a range of 500 mV. Incredibly, the potential is shifted so far cathodically in the PCy_3 adduct that the $Ru_2^{6+/5+}$ couple becomes accessible and for the first time in diruthenium tetracarboxylate chemistry a fully oxidized $[Ru_2(\mu\text{-}O_2CR)_4L_2]^{2+}$ species was reversibly generated [7]. Despite the 500 mV decrease in the $E_{1/2}$ for the $Ru_2^{5+/4+}$ couple the near-degeneracy of the $(\pi^*\delta^*)^3$ HOMO is not lifted as the magnetic moments, μ, per Ru_2 are all relatively constant at 4.2 B.M., indicating three unpaired electrons in all cases. It was concluded that the π^* and δ^* orbitals vary their energies significantly but move, essentially, in tandem. This allows for selective redox tuning of the metal centers without affecting their magnetic and, to a certain extent, their spectroscopic properties. It should be noted that the correlation of $E_{1/2}$ with DN values is, to a certain extent, limited. It would be interesting to correlate

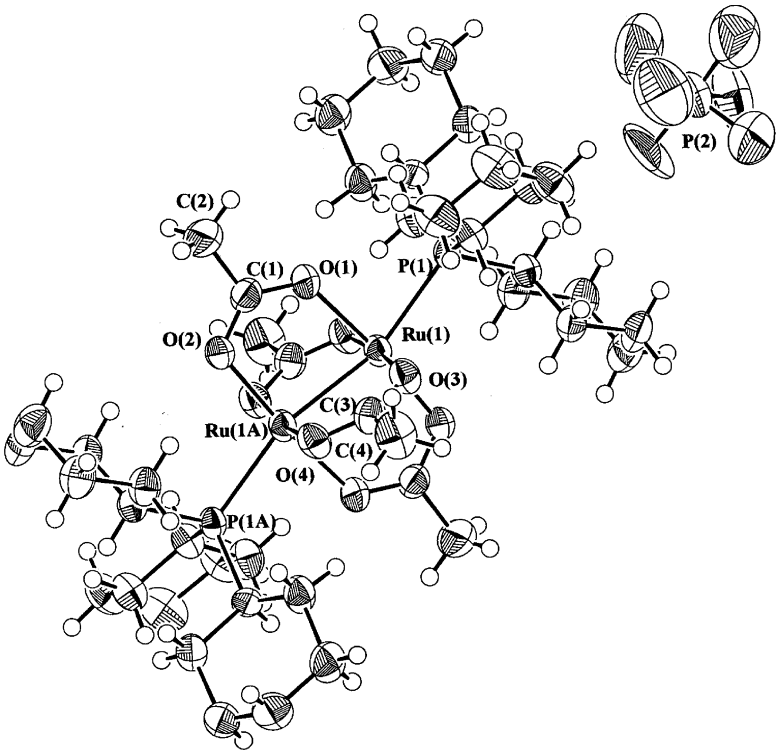

Fig. 1. Structure of $[Ru_2(\mu\text{-}O_2CCH_3)_4(PCy_3)_2](PF_6)$.

not only $E_{1/2}$ values but other physical properties with other, more specific, ligand parameters such as Drago's calorimetric E and C parameters or Lever's electrochemical based E_L parameters.

2.2. Complexes with biologically relevant axial ligands

A few of the complexes highlighted in the previous section have axial ligands that could be deemed to have some biological relevance. The urea adduct [4] shows an interesting property in that it crystallizes as a rare co-adduct system from 1-propanol in which both $[Ru_2(\mu\text{-}O_2CCH_3)_4(urea)_2]^+$ and $[Ru_2(\mu\text{-}O_2CCH_3)_4(1\text{-propanol})_2]^+$ cations are present in the unit cell. One important aspect of investigating the binding of biologically relevant ligands is the nature of any hydrogen bonding that may occur. The urea derivative shows a weak hydrogen bond (3.18 Å) between the urea nitrogen and an acetate oxygen on an adjacent $[Ru_2(\mu\text{-}O_2CCH_3)_4(1\text{-propanol})_2]^+$ unit as well as a stronger interaction (2.78 Å) between the 1-propanol oxygen and an acetate oxygen on the $[Ru_2(\mu\text{-}O_2CCH_3)_4(urea)_2]^+$ cation.

Sudha and Chakravarty [10] synthesized and structurally characterized a 2-methylimidazole (2-mimH) adduct, $[Ru_2(\mu\text{-}O_2CC_6H_4\text{-}p\text{-}OCH_3)_4(2\text{-mimH})_2](ClO_4)\cdot 1.75CH_2Cl_2\cdot H_2O$. This compound showed bond lengths and angles typical of $[Ru_2(\mu\text{-}O_2CR)_4(L)_2]^+$ type complexes with the 2-mimH binding through the imine nitrogen. A weak hydrogen bond (3.06 Å) is noted between the amine nitrogen and an oxygen on the perchlorate anion.

Recent work in our lab has centered on the synthesis, characterization and hydrogen-bonding aspects of adducts containing nucleotide bases and their purine and pyrimidine analogues. A preliminary structural paper [11] showed the trans/anti coordination of two quinoline ligands to the Ru_2(II,III) tetraacetate core (Fig. 2). Here, we see weak but definite C–H···O hydrogen bonds between two of the ring carbons and the four facing oxygen atoms on the bridging acetates. The C···O distances range from 3.15 to 3.26 Å. In more current work, we have seen similar ligand binding behaviour but more extensive hydrogen-bonding interactions in imidazole, azaindole and caffeine diadducts [12].

2.3. Weakly coordinating ligands

In many cases, diadducts of diruthenium tetracarboxlates are obtained by the dechlorination of $Ru_2(\mu\text{-}O_2CR)_4Cl$ (normally with Ag^+ or Tl^+) in a donor solvent resulting in the formation of $[Ru_2(\mu\text{-}O_2CR)_4L_2]^+$ adducts with L being a modest to strong Lewis base. Cotton has carried out these dechlorination reactions in non-coordinating solvents such as dichloromethane, CH_2Cl_2, in the presence of weakly coordinating anions such as ClO_4^- or BF_4^- (despite very limited solubilities of the reactants) and has found that these too will bind axially to the diruthenium core [13]. For example, the reaction of $Ru_2(\mu\text{-}O_2CEt)_4Cl$ with ClO_4^- produces the infinite one-dimensional chain, $\{Ru_2(\mu\text{-}O_2CEt)_4(ClO_4)\}_\infty$, with the ClO_4^- ion bridging adjacent $Ru_2(\mu\text{-}O_2CEt)_4^+$ units (Fig. 3) in a fashion similar to the parent, $Ru_2(\mu\text{-}O_2CEt)_4Cl$,

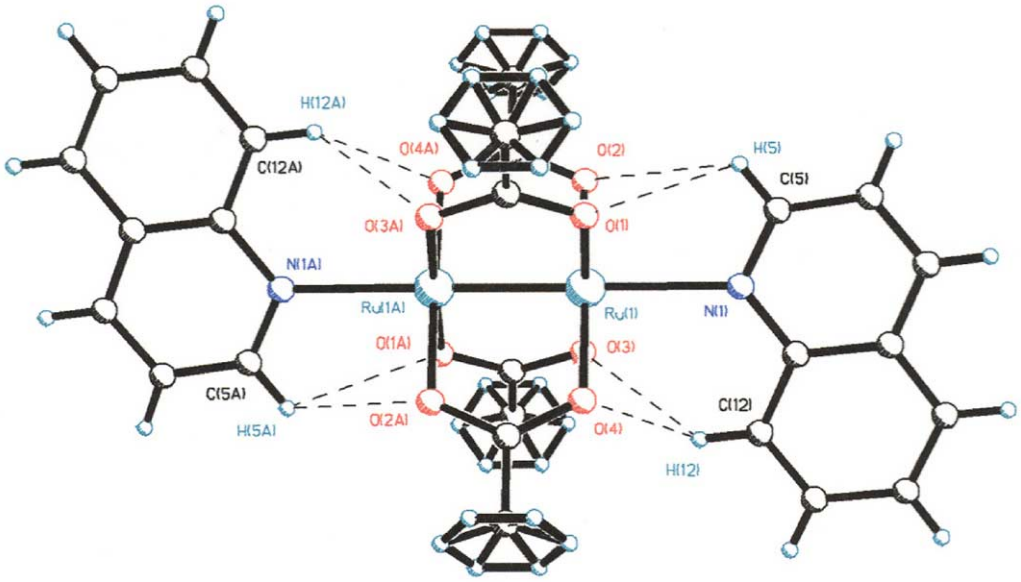

Fig. 2. Structure of the $[Ru_2(\mu\text{-}O_2CCH_3)_4(quinoline)_2]^+$ cation showing the intramolecular C—H · · · O hydrogen bonds. There is disorder in the methyl groups.

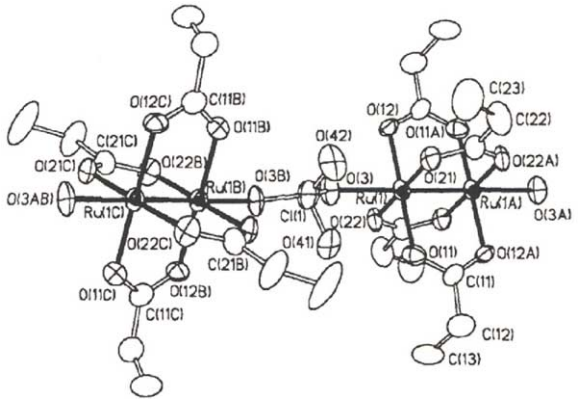

Fig. 3. Structure of the $\{Ru_2(\mu\text{-}O_2CEt)_4(ClO_4)\}_\infty$ chain complex. Reproduced from [13], with permission of the copyright holders.

compound. A similar chain is formed with $CF_3SO_3^-$. Reaction of $Ru_2(\mu\text{-}O_2CR)_4Cl$ (R = Me or Et) with BF_4^- produced $[Ru_2(\mu\text{-}O_2CR)_4][BF_4]$, however, no structures were obtained and direct evidence for a monodentate or bridging binding mode of the BF_4^- could not be verified. Subsequent reaction of $[Ru_2(\mu\text{-}O_2CCH_3)_4][BF_4]$ with pyridine did produce the structurally characterized $(py)Ru_2(\mu\text{-}O_2CCH_3)_4(BF_4)$ in which the BF_4^- is monodentately bound.

3. Novel equatorial adducts

3.1. Ru_2(II,III) complexes with chiral bridging carboxylates

McCann et al. [14] synthesized a series of Ru_2(II,III) complexes incorporating the racemic and chiral forms of *endo*/*exo*-bicyclo[2.2.1]hept-5-ene-2-carboxylate as the bridging ligand. Metathesis of $Ru_2(\mu\text{-}O_2CCH_3)_4Cl$ with the appropriate form of the acid yielded the tetracarboxylate complexes $[Ru_2\{(\pm)\text{-}exo\text{-}\mu\text{-}O_2CC_7H_9\}_4Cl]$, $[Ru_2\{(\pm)\text{-}endo\text{-}\mu\text{-}O_2CC_7H_9\}_4Cl]\cdot H_2O$ and $[Ru_2\{(-)\text{-}endo\text{-}\mu\text{-}O_2CC_7H_9\}_4Cl]\cdot H_2O$. The reaction of $[Ru_2\{(\pm)\text{-}endo\text{-}/(\pm)\text{-}exo\text{-}\mu\text{-}O_2CC_7H_9\}_4Cl]$ with $Ag\{(\pm)\text{-}endo\text{-}/(\pm)\text{-}exo\text{-}\mu\text{-}O_2CC_7H_9\}$ and $Ag(O_2CCF_3)$ yielded the mixed-acid pentacarboxylates $[Ru_2\{(\pm)\text{-}endo\text{-}/(\pm)\text{-}exo\text{-}\mu\text{-}O_2CC_7H_9\}_5]\cdot 2H_2O$ and $[Ru_2\{(\pm)\text{-}endo\text{-}/(\pm)\text{-}exo\text{-}\mu\text{-}O_2CC_7H_9\}_4(\mu\text{-}CF_3CO_2)]$, respectively. Finally, metathesis of $[Ru_2(\mu\text{-}O_2CCH_3)_4(O_2CCH_3)_2H]\cdot 0.7H_2O$ with the appropriate acid yielded the pentacarboxylates, $[Ru_2\{(\pm)\text{-}exo\text{-}\mu\text{-}O_2CC_7H_9\}_5]$, $[Ru_2\{(\pm)\text{-}endo\text{-}\mu\text{-}O_2CC_7H_9\}_5]$, and $[Ru_2\{(-)\text{-}endo\text{-}\mu\text{-}O_2CC_7H_9\}_5]$. While the only structurally characterized complex with this ligand to be reported was a Cu_2(II,II) analogue, all of the diruthenium complexes were identified using elemental analysis, magnetic susceptibility, IR and UV–vis spectroscopy, molar conductivity and FAB mass spectrometry. It was assumed that the chiral integrity is maintained (for those complexes made from resolved ligands) throughout the exchange reactions. All of the complexes were found to be soluble in methanol, ethanol, THF and acetone.

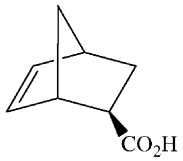

bicyclo[2.2.1]hept-5-ene-2-carboxylic acid

3.2. Ru_2(II,III) complexes incorporating metallocenecarboxylates

Exchange of the equatorial carboxylates with metal-containing carboxylates such as ferrocene and ruthenocene

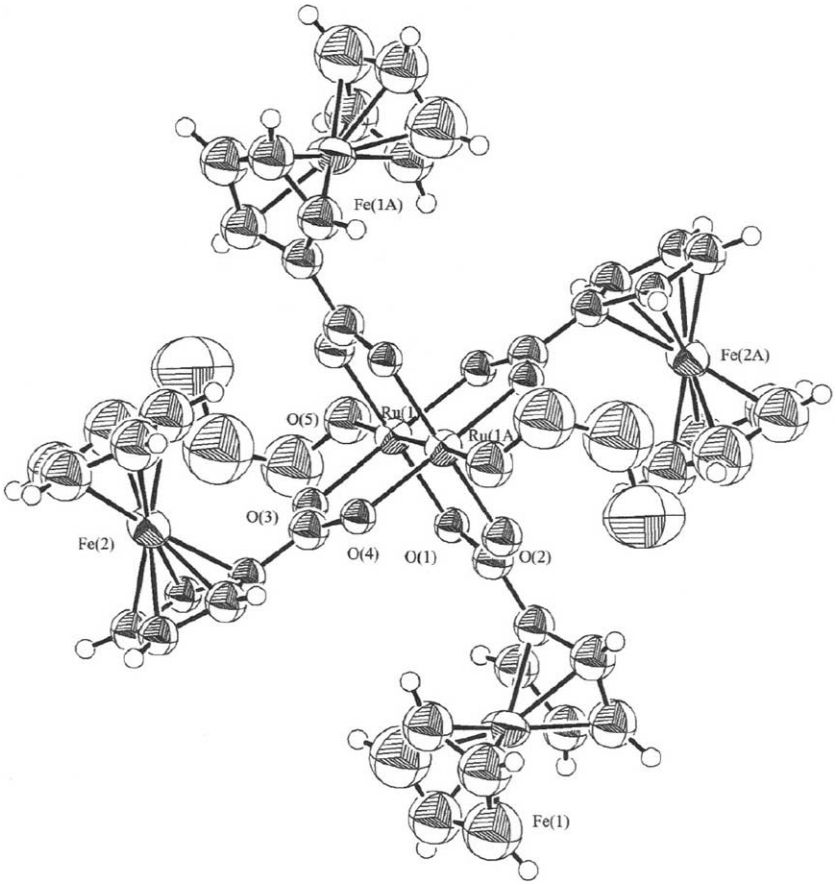

Fig. 4. Structure of the $[Ru_2(\mu\text{-}O_2CC_5H_4FeC_5H_5)_4(n\text{-}PrOH)_2]^+$ cation.

carboxylic acids has been carried out in our lab in order to investigate their structural and redox properties [15,16]. Very few metal complexes with metallocene carboxylate ligands appear in the literature despite the fact that they offer a unique example for studying possible interactions between "inorganic" and "organometallic" metal centers which has not been explored to any great extent. A series of both chloro, $Ru_2(\mu\text{-}O_2C(X)Mc)_4Cl$, and alcohol diadduct, $[Ru_2(\mu\text{-}O_2C(X)Mc)_4(ROH)_2](PF_6)$, derivatives were synthesized, where Mc = Fc (ferrocenyl) and X = nothing, $–CH_2–$, $–(CH_2)_2–$, $–(CH_2)_3–$ and –CH=CH– (with R = Me, Et or *n*-Pr) or Mc = Rc (ruthenocenyl) and X = nothing (with R = *n*-Pr). X-ray structures of three of the diadducts, $[Ru_2(\mu\text{-}O_2CFc)_4(n\text{-}PrOH)_2](PF_6)$ (Fig. 4), $[Ru_2(\mu\text{-}O_2CCH{=}CHFc)_4(n\text{-}PrOH)_2](PF_6)$, and $[Ru_2(\mu\text{-}O_2CRc)_4(n\text{-}PrOH)_2](PF_6)$ were reported. The latter is the first structurally characterized example of a metal complex with a ruthenocene carboxylate ligand.

Cyclic voltammetry (CV) and Osteryoung square-wave voltammetry (OSWV) measurements on $[Ru_2(\mu\text{-}O_2CFc)_4(n\text{-}PrOH)_2](PF_6)$ showed there to be a small but significant interaction between the irons in the ferrocenyl groups. The cyclic voltammogram showed two distinct ferrocenyl-centered cathodic and anodic peaks (each peak consisting of two closely overlapping one-electron transfer processes). A similar peak splitting was seen in the OSWV. These separations ranged from 75 to 90 mV and corresponded to the generation of a multiple-mixed valent state that contained a Ru_2(II,III) core along with two Fe(II) and two Fe(III) centers. The through-bond distance between the iron centers was 13.5 Å. Similar measurements made on the $[Ru_2(\mu\text{-}O_2CCH{=}CHFc)_4(n\text{-}PrOH)_2](PF_6)$ complex showed no evidence of splitting in the CV (although peak broadening was evident) but a splitting of 41 mV was observed in the OSWV. This is close to the statistical limit of 35.6 mV for a non-interacting system but may still indicate a very small interaction even over the relatively large Fe–Fe distance of 19.3 Å. No interactions are seen in the compounds with the longer, saturated spacers. Unfortunately, the ruthenocenyl derivative, $[Ru_2(\mu\text{-}O_2CRc)_4(n\text{-}PrOH)_2](PF_6)$, displayed only an irreversible Rc centered oxidation wave corresponding to a total of eight electrons (four two-electron transfers).

3.3. Ru_2(II,II) complexes

Far fewer complexes (axially or equatorially substituted) have been made of the reduced, air-sensitive, Ru_2(II,II) form. Using zinc amalgam under a nitrogen atmosphere in tetrahydrofuran (thf), Barral et al. [17] were able to reduce $Ru_2(\mu\text{-}O_2CR)_4Cl$ to afford the various equatorially substituted thf

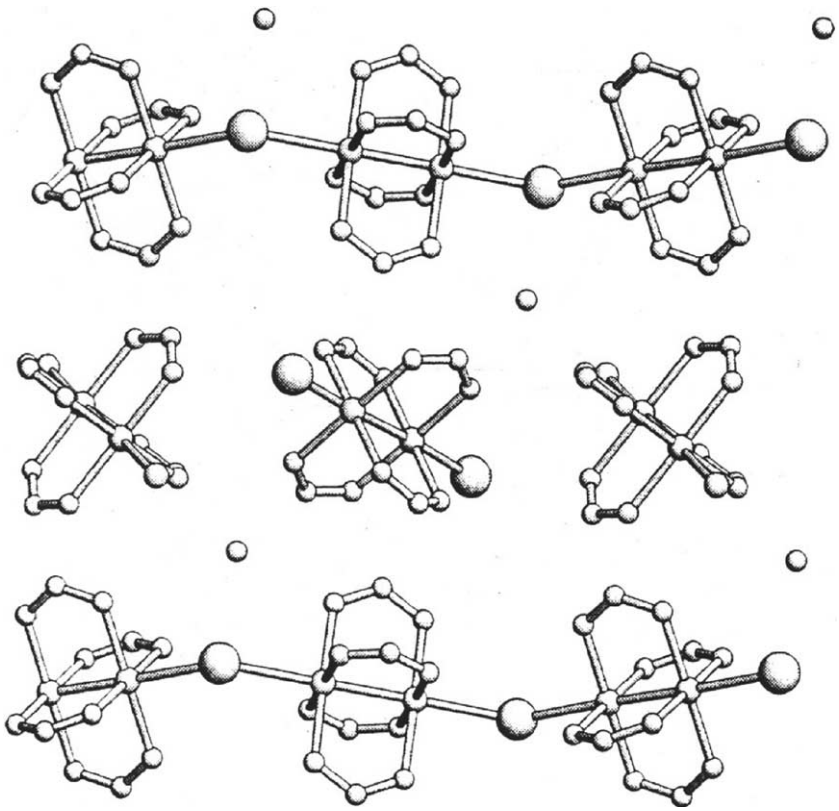

Fig. 5. Arrangement in the solid state of the complex with stoichiometry, $[Ru_2(\mu\text{-}O_2CCH_2OEt(Cl)(H_2O)]$. Reproduced from [18], with permission of the copyright holders.

adducts $Ru_2(\mu\text{-}O_2CR)_4(thf)_2$ (where R = Me, Ph, C_6H_4-*o*-Cl, C_6H_4-*p*-CMe_3, $CHMe_2$, CMe_3 and $CHEt_2$). These rapidly lose the axial thf molecules in vacuo to yield the unsolvated species. (Again, as mentioned earlier, no truly unsolvated or unligated species exists as there will always be weak interactions with the carboxylate oxygen atoms of neighbouring dimers to form oligomers.) Axial diadducts could be reformed by reaction with MeOH, thf or $OPPh_3$. It was noted that the reaction of $Ru_2(\mu\text{-}O_2CMe)_4Cl$ with phenylglyoxylic acid ($HO_2CC(O)Ph$) lead directly to the reduced $Ru_2(\mu\text{-}O_2CC(O)Ph)_4$ product as well as an unidentified, presumably oxidized, residue. This reaction was postulated to proceed via a disproportionation pathway since the yield of the reduced product was less than 50% and because of the presence of an oxygen atom close to the carboxyl group. Similar behaviour has been seen in the past whenever there was a donor atom on the α carbon to the carboxyl group of the exchanging carboxylic acid.

4. Polymers and extended structures

In this section, we review those compounds which lead to an extended array structure but where the study of their magnetic properties was not the major focus. In the next section, a large number of polymers and extended assemblies are discussed in terms of their interesting magnetism.

Most complexes of the type $Ru_2(\mu\text{-}O_2CR)_4X$ form halide(X)-bridged, linear or zig-zag chains, depending on the nature of R. However, in some cases, discrete molecular units of the form $Ru_2(\mu\text{-}O_2CR)_4(Cl)(S)$, where S = H_2O or thf, are also known to form. Barral et al. have investigated this dependence on R further and found that both polymeric and ionic forms of these complexes can be present *at the same time* in solution and in the solid state [18]. They synthesized an unprecedented complex, with ethoxyacetate as the bridging ligand, of stoichiometry $Ru_2(\mu\text{-}O_2CCH_2OEt)_4(Cl)(H_2O)$ and found it to have not only $Ru_2(\mu\text{-}O_2CCH_2OEt)_4Cl$ zig-zag chains (the Ru–Cl–Ru angle = 138.4°) but also discrete $[Ru_2(\mu\text{-}O_2CCH_2OEt)_4(H_2O)_2]^+$ cations and $[Ru_2(\mu\text{-}O_2CCH_2OEt)_4(Cl)_2]^-$ anions (Fig. 5). The chains alternate with cationic-anionic units that are held together by electrostatic forces. The only difference between this complex and other polymeric systems involving $Ru_2(\mu\text{-}O_2CR)_4Cl$ units is the presence of the oxygen in the carboxylate chain which the authors suggest may have some influence on the packing in the solid state. Subsequent reaction of the complex with $OPPh_3$ leads to the formation of the discrete mixed-diadduct $Ru_2(\mu\text{-}O_2CCH_2OEt)_4(Cl)(OPPh_3)$.

When *trans*-2-methyl-2-pentenoate is used as the bridging carboxylate a linear polymer, $[Ru_2(\mu\text{-}O_2CC(Me)=CHEt)_4Cl]_n$, is formed in the solid state but the complex appears to be non-polymeric in solution [19]. From its solubility properties in a variety of solvents

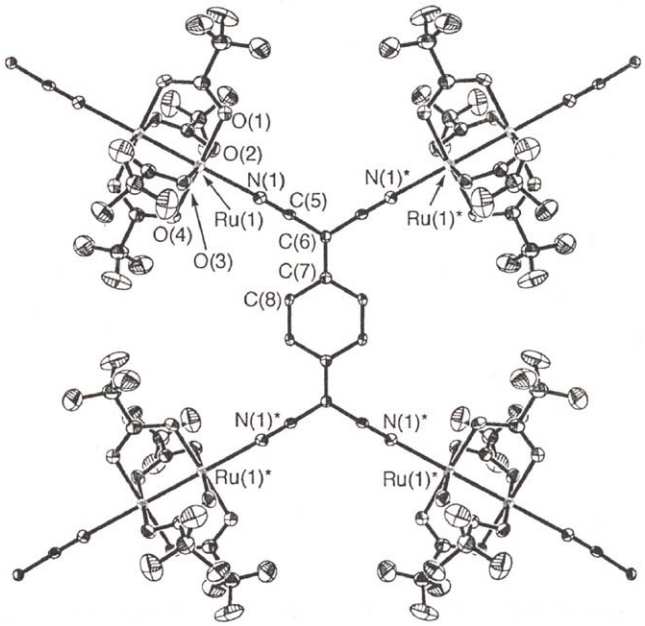

Fig. 6. Diagram showing structure of one TCNQ ligand coordinated to four independent $[Ru_2(\mu\text{-}O_2CCF_3)_4]$ units. Reproduced from [20], with permission of the copyright holders.

(S) and its conductivity in solution it was suggested that discrete $Ru_2(\mu\text{-}O_2CC(Me)=CHEt)_4(Cl)(S)$ units were present. The reaction with $OPPh_3$ to yield $Ru_2(\mu\text{-}O_2CC(Me)=CHEt)_4(Cl)(OPPh_3)$ would seem to confirm this and the reaction with SCN^- yields a polymer again in the solid state with bridging SCN^- groups.

A two-dimensional network structure incorporating $[Ru_2(\mu\text{-}O_2CCF_3)_4]$ units and 7,7,8,8-tetracyanoquinodimethane (TCNQ) bridges, $[\{Ru_2(\mu\text{-}O_2CCF_3)_4\}_2(\mu_4\text{-TCNQ})\cdot 3(C_7H_8)]_\infty$, was synthesized by Dunbar and coworkers from toluene [20] and appears to show significant electronic delocalization (Fig. 6). The 2-D sheets are separated by 6.6 Å with the toluene molecules of solvation lying between these layers. Evidence for this delocalization came from the IR and visible spectra of the complex which showed characteristic features of a partially reduced TCNQ with concomitant oxidation of one or more of the Ru_2(II,II) units to the Ru_2(II,III) form due to significant M–L π-backbonding. Also, from the X-ray structure of the complex, the bond lengths within the TCNQ ligands in the complex are intermediate between the values of "free" $TCNQ^0$ and $TCNQ^-$, an indication of partial reduction.

5. Magnetic properties

By far the most studied aspect of diruthenium tetracarboxylates, particularly in the (II,III) mixed-valent derivatives, has been their magnetic properties. The following subsections outline those complexes that were studied essentially for their magnetic properties. Compounds that were studied primarily for their mesomorphic properties but that also displayed interesting magnetic behaviour are discussed in Section 6.

5.1. Nitroxide radical derivatives

Mentioned in our previous review, Handa and coworkers [21–26] have continued their studies on diruthenium(II,III) pivalate dimers linked by various nitroxide radical derivatives. The purpose behind these studies was to try to generate chains that exhibited ferrimagnetic properties by the coupling of the alternating spin $S_1 = 3/2$ from the (II,III) dimer and $S_2 = 1/2$ from the nitroxide radical. Earlier studies on $[Ru_2(\mu\text{-}O_2CCMe_3)_4(tempo)_2][Ru_2(\mu\text{-}O_2CCMe_3)_4(H_2O)_2(BF_4)_2$, where tempo = 2,2,6,6-tetramethylpiperidine-1-oxyl, had already shown strong ferrimagnetic interactions between the Ru_2 cation and nitroxide radical [27].

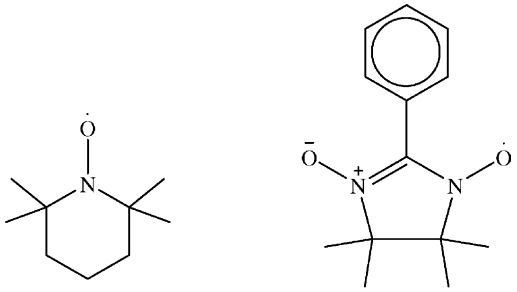

tempo nitph

The chain complex $[Ru_2(\mu\text{-}O_2CCMe_3)_4(nitph)]_n(BF_4)_n$ (nitph = 2-phenyl-4,4,5,5-tetramethyl-4,5-dihydro-1*H*-imidazol-1-oxyl-3-*N*-oxide) was crystallographically characterized and studied by variable temperature magnetic susceptibility [21]. The complex displays a zig-zag chain with the nitronyl–nitroxide radical bridging adjacent Ru_2(II,III) units through its oxygen atoms. The magnetic data turned out to be rather complicated and data-fitting to an alternating ferromagnetic chain model of $S_1 = 3/2$ and $S_2 = 1/2$ spins was hampered by a large zero-field splitting (ZFS) term intrinsic to the Ru_2(II,III) center. Unfortunately, inclusion of the zero-field splitting made the problem intractable and a simplification using a spin pair model had to be made (Scheme 1).

This model assumes that the only significant coupling (J_{M-R} value) occurs between one end of the nitroxide radical and one of the Ru atoms and that the coupling at the other end is negligible ($J'_{M-R} = 0$). Using this model a decent fit to the observed data was found and a coupling constant

$$\underset{S_1 = 3/2}{J_{M\text{-}R}} \text{ ------- (Ru2-Ru1) ------- } \underset{S_2 = 1/2}{J'_{M\text{-}R} = 0} \text{ ------- (nitph) ------- } \underset{S_1 = 3/2}{J_{M\text{-}R}} \text{ ------- (Ru2-Ru1) ------- } \underset{S_2 = 1/2}{J'_{M\text{-}R} = 0} \text{ ------- (nitph) ------- } J_{M\text{-}R}$$

Scheme 1. Spin-pair model for magnetic exchange in chain complexes.

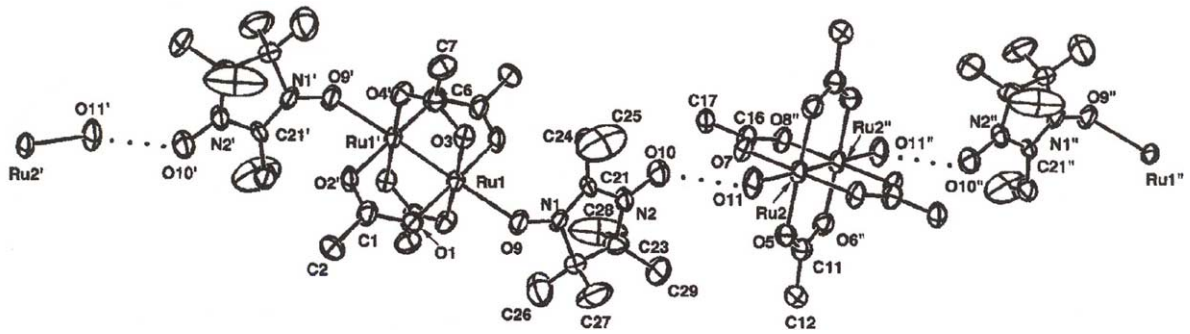

Fig. 7. Structure of the $[\{Ru_2(\mu\text{-}O_2CCMe_3)_4(nitet)_2\}\{Ru_2(\mu\text{-}O_2CCMe_3)_4(H_2O)_2\}]_n\text{-}(BF_4)_{2n}\cdot 2nCH_2Cl_2$ chain. The methyl groups on the pivalate ions, CH_2Cl_2 molecules and BF_4^- ions were omitted for clarity. Reproduced from [24], with permission of the copyright holders.

of $J_{M-R} = -100\,cm^{-1}$, and a zero-field splitting parameter of $D = 65\,cm^{-1}$, were obtained. (The D value is similar to values obtained for analogous systems in the past.) In order to justify the use of this model and $J'_{M-R} = 0$ the authors compared the differences in the bonding features at the two axial sites. The Ru_2–O–N bond angle of 147.5(7)° is very similar to the Ru–O–N axial bond angles in the tempo derivative mentioned above which showed a $J_{M-R} = -130\,cm^{-1}$. However, the Ru_1–O–N angle is only 131.7(7)° and was deemed inappropriate for significant interaction between the Ru_2 core and the radical via a π-pathway mechanism. As well, the Ru_1–O distance of 2.264(8) Å is significantly longer than the Ru_2–O distance of 2.236(8) Å making interactions even more unfavourable. A σ-pathway mechanism was considered to be unfavourable on either side. The authors do not rule out the possibility that J'_{M-R} could have a finite value (indeed from calculations of overlap integrals between the magnetic orbitals they state that $|J'_{M-R}|$ could be as high as $33\,cm^{-1}$) however, the large zero-field splitting in comparison with J'_{M-R} is the reason why the spin pair model seemed to work. (A calculation based on a molecular field approximation was also performed by the authors but the fittings could not be made when J'_{M-R} had any finite value.)

Quite a different story is played out when the nitroxide radical is 2-(4-pyridyl)-4,4,5,5-tetramethyl-4,5-dihydro-1*H*-imidazolyl-1-oxyl-3-*N*-oxide (*p*-nitpy). The complex $[Ru_2(\mu\text{-}O_2CCMe_3)_4(p\text{-nitpy})]_n(BF_4)_n$ displays ferromagnetic behaviour [22]. The crystal structure reveals an extended zig-zag chain with the nitronyl–nitroxide bridging through the pyridyl nitrogen and an oxygen on the nitroxide. The magnetic susceptibility measurements show an increase in the magnetic moment as the temperature is lowered, and reaches a maximum at 8 K. The data fitting gave a value of $J_{M-R} = 20\,cm^{-1}$ and $J'_{M-R} = 0.45\,cm^{-1}$ (J_{M-R} being the spin coupling constant between the Ru and radical through the N–O group and J'_{M-R} the value between the other Ru through the pyridyl group) and $D = 50\,cm^{-1}$. In this case, the Ru_1–O–N bond angle is 125.3(6)°, considerably smaller than in the case of the nitph derivative above, and brings about an orthogonality between the Ru π* and nitroxide π* orbitals which leads to the ferromagnetic behaviour.

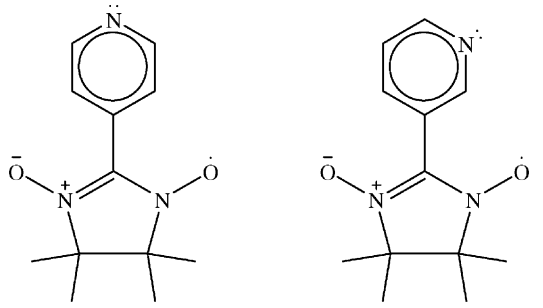

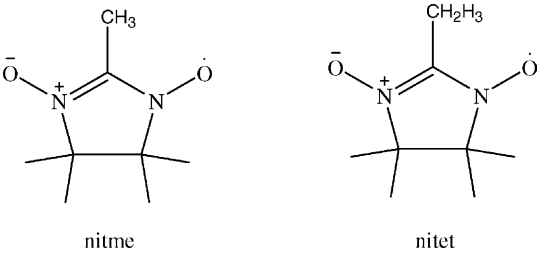

Novel chain compounds in which nitroxide radical adducts and diaquo adducts of diruthenium(II,III) tetrapivalate are linked via hydrogen bonds, similar to the tempo derivative, have also been investigated. The mixed-adduct chain complexes $[(Ru_2(\mu\text{-}O_2CCMe_3)_4(L)_2)(Ru_2(\mu\text{-}O_2CCMe_3)_4(H_2O)_2)]_n(BF_4)_n$ where L = 2,4,4,5,5-pentamethyl-4,5-dihydro-1*H*-imidazolyl-1-oxyl-3-*N*-oxide (nitme) and L = 2-ethyl-4,4,5,5-tetramethyl-4,5-dihydro-1*H*-imidazolyl-1-oxyl-3-*N*-oxide (nitet) consist of $[Ru_2(\mu\text{-}O_2CCMe_3)_4(L)_2]^+$ and $[Ru_2(\mu\text{-}O_2CCMe_3)_4(H_2O)_2]^+$ cations linked together via hydrogen bonds between N–O nitroxide groups and axial water molecules with an O–O distance of 2.78–2.81 Å [23,24] (Fig. 7). In this case, the two ruthenium atoms in the nitroxide adduct cations are crystallographically equivalent and hence any magnetic interactions between the Ru and the nitroxide would be the same and is defined as J_{M-R}. Interactions between nitroxides on the same adduct through the Ru–Ru bond are defined as J_{R-R} with no significant weight given to interactions with the diaquo adducts through the hydrogen bond (Scheme 2).

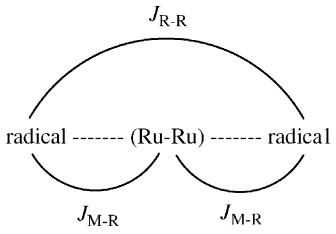

Scheme 2. Magnetic exchange model for radical-Ru_2-radical adduct complexes.

The magnetic moment for both compounds increases slightly from room temperature to 140 K, remains essentially constant to 100 K, and then gradually decreases down to 2 K. Using the van Vleck equation based on the Heisenberg model (Scheme 2), $J_{M–R} = 20\ cm^{-1}$ (for both compounds) and $J_{R–R} = -50\ cm^{-1}$ (for nitme) and $-47\ cm^{-1}$ (for nitet). A ferromagnetic interaction therefore occurs between the Ru_2(II,III) core and the nitroxide radical and an antiferromagnetic interaction is seem between the two nitroxides through the metal–metal bond. The Ru–O–N bond angles of 121.5(6)° (nitme) and 122.5(7)° (nitet) lead to orthogonality of the magnetic orbitals (Ru π^* or δ^* and nitroxide π^*) as was seem above in the *p*-nitpy derivative and explains the ferromagnetic coupling. The close to 120° angle is also suitable for antiferromagnetic interactions through σ or σ^* orbitals of the Ru–Ru core between the nitroxides. ESR measurements supported this conclusion.

In addition to chain structures, in which the nitroxides act as bridges, discrete nitroxide diadducts have also been synthesized by using an excess of the radical ligand [25]. Two bis-adduct complexes of the form $[Ru_2(\mu\text{-}O_2CCMe_3)_4(L)_2]X$ where L = 2-(3-pyridyl)-4,4,5,5-tetramethyl-4,5-dihydro-1*H*-imidazolyl-1-oxyl 3-*N*-oxide (*m*-nitpy) or *p*-nitpy and X = BF_4^- or BPh_4^- show coordination of the pyridyl group to the Ru_2(II,III) core only (contrast the pyridyl nitrogen and oxyl oxygen coordination in the *p*-nitpy chain complex mentioned earlier). The magnetic moments for the two complexes (with either counterion) show essentially non-interacting spins ($S = 3/2$ on the Ru_2(II,III) core and two $S = 1/2$ spins on the nitroxides) at room temperature (μ_{eff} = 4.7–5.0 B.M.) and a steady decrease in μ_{eff} as the temperature is lowered, indicative of the strong zero-field splitting. However, there are differences in when the two complexes begin to show this decrease in μ_{eff}. For the *m*-nitpy derivative, a sharp decrease begins at about 50 K whereas it does not occur until ca. 5 K for the *p*-nitpy analogue. With this in mind a closer look at the intramolecular interactions, shown in Scheme 2, as well as the through-space intermolecular interaction between nitroxides of neighbouring cation units ($J_{R\cdots R}$), was needed. The intramolecular interaction between nitpy groups within the same adduct (through the Ru–Ru center), $J_{R–R}$, was deemed to be too weak to be significant and set to $0\ cm^{-1}$. A molecular-field approximation was applied (as had been done successfully before) to the remaining interactions, $J_{M–R}$ and $J_{R\cdots R}$, with the assumption that one was considerably smaller than the other. Assuming $|J_{R\cdots R}| \ll |J_{M–R}|$ lead to good fits of the data for the *m*-nitpy derivative with $J_{M–R} = -1.0\ cm^{-1}$ ($J_{R\cdots R} = 0\ cm^{-1}$) for both X = BF_4^- and BPh_4^-. For the *p*-nitpy derivative the intermolecular interactions seem to dominate and better fits were obtained under the condition $|J_{M–R}| \ll |J_{R\cdots R}|$ with $J_{R\cdots R} = -5.0\ cm^{-1}$ ($J_{M–R} = 0.8\ cm^{-1}$) for X = BF_4^- and $J_{R\cdots R} = -6.0\ cm^{-1}$ ($J_{M–R} = 1.4\ cm^{-1}$) for X = BPh_4^-. In this case, the $J_{M–R}$ values are non-zero but small and positive. The reason for this was postulated to be due to a spin-polarization mechanism. Due to the large dihedral angle (ca. 30°) between the pyridyl ring and the ONCNO plane of the nitroxide and the *odd* number of atoms (an *even* number for the *m*-nitpy derivative) between the paramagnetic Ru_2(II,III) core and the N–O group, spin polarization would lead to a net ferromagnetic spin-exchange (recall the weak ferromagnetism, $J_{M–R} = 0.45\ cm^{-1}$, in the *p*-nitpy chain complex). The reason for the larger $J_{R\cdots R}$ values in the *p*-nitpy adduct was unclear.

Diadducts of the nitme and nitet nitroxides were also prepared [24]. In both of these cases, the intramolecular coupling was greater than in the nitpy adducts (presumably because there was no intervening pyridyl ring). Ferromagnetic coupling occurred between the Ru_2(II,III) core and the nitroxide with $J_{M–R} = 5\ cm^{-1}$ for both adducts and antiferromagnetic coupling between nitroxides on the same dimer with $J_{R–R} = -40\ cm^{-1}$. The positive $J_{M–R}$ is due to the small Ru–O–N bond angle of 123.7(4)° in the nitme adduct. (No structure was reported for the nitet adduct but one could assume a similar angle.)

A mixed di-adduct complex of diruthenium(II,III) tetrapivalate in which one axial site is occupied by nitph and the other by water showed ferrimagnetic coupling between the Ru_2(II,III) core and the axial nitroxide with $J_{M–R} = -45\ cm^{-1}$ [26]. Here, any intradimer radical–radical interactions are excluded and only the pure Ru_2(II,III)-radical π^* interaction is manifest. (Hydrogen bonds do link adjacent dimers via axial water–BF_4^- counterion–axial water interactions but were deemed not to mediate any significant interaction.) The slightly diminished coupling was due to the smaller Ru–O–N bond angle of 137.7(5)° (compare $J_{M–R} = -100$ when the angle was 147.5(7)° in the nitph chain complex).

It appears very clear from all of Handa's work that the nature and magnitude of the spin-exchange ($J_{M–R}$ and/or $J_{R–R}$) is dictated by the axial Ru–O–N bond angle. A summary of all relevant coupling constants and the corresponding bond angles is given in Table 2. Smaller bond angles (<130°) favour larger antiferromagnetic $J_{R–R}$ values due to σ or σ^* orbitals of the Ru_2(II,III) core overlapping with the π^* orbital on the axial nitroxide and modest ferromagnetic $J_{M–R}$ values due to the orthogonality of the respective π (or π^*) orbitals between the core and the ligand whereas the larger bond angles (>135°) favour ferrimagnetic $J_{M–R}$ values due to an increased π^* orbital overlap between the core and the π^* orbital on the axial nitroxide with no substantial intraradical coupling ($J_{R–R}$).

Table 2
Ru–O–N bond angles and J values for axially O-bonded nitroxide complexes of $[Ru_2(\mu\text{-}O_2CR)_4]^{+/0}$

Complex	Ru–O_{ax}–N (°)	J_{M-R} (cm^{-1})	J_{R-R} (cm^{-1})
$[\{Ru_2(O_2CCMe_3)_4(nitme)_2\}\{Ru_2(O_2C\text{-}CMe_3)_4(H_2O)_2\}]_n(BF_4)_{2n}\cdot 2nCH_2Cl_2$	121.5(6)	20	−50
$[\{Ru_2(O_2CCMe_3)_4(nitet)_2\}\{Ru_2(O_2C\text{-}CMe_3)_4(H_2O)_2\}]_n(BF_4)_{2n}\cdot 2nCH_2Cl_2$	122.5(7)	20	−47
$[Ru_2(O_2CCMe_3)_4(nitme)_2](BF_4)\cdot 2CH_2Cl_2$	123.7(4)	5	−40
$[Ru_2(O_2CCMe_3)_4(p\text{-nitpy})]_n(BF_4)_n$	125.3(6)	20	–[a]
$[Ru_2(O_2CCMe_3)_4(nitph)(H_2O)](BF_4)$	137.7(5)	−45	–[a]
$[Ru_2(O_2CCMe_3)_4(tempo)_2][Ru_2(O_2C\text{-}CMe_3)_4(H_2O)_2](BF_4)_2$	151.5(3)	−130	0
$[Ru_2(O_2CCF_3)_4(tempo)_2]$	158.2(3)	−263	0
$[Ru_2(O_2CCMe_3)_4(nitph)_n](BF_4)_n$	131.7(7)	0	–[b]
	147.5(7)	−100	0

[a] One of the two axial sites of the Ru_2(II,III) core is only coordinated by the N–O group of the radical.
[b] One (147.5(7)°) of the two axial bond angles is not suited for operating the radical–radical interaction, resulting in no observed interaction between the radicals.

5.2. Other organic-bridge derivatives

Another potential radical bridge that has been quite popular in mediating spin-exchange is 7,7,8,8-tetracyanoquinodimethane (tcnq) which was mentioned earlier in the context of Dunbar's work and electronic delocalization. Handa et al. synthesized the "dimer-of-dimers", $[(Ru_2(\mu\text{-}O_2CCMe_3)_4)_2(\mu\text{-tcnq})(H_2O)_2](BF_4)_2$, in which the tcnq bridges through two of the trans cyano groups with water molecules occupying the other axial sites of the Ru_2 core [28]. From the crystallographic evidence, the tcnq molecule was found to be neutral and that the Ru_2 dimers maintain their (II,III) valence state. The magnetic moment for this complex drops off as the temperature is lowered with most of the decrease being due to the large zero-field splitting (D = 65 cm^{-1}), however, a very small antiferromagnetic interaction between the Ru_2(II,III) cores of the adjacent dimers (J_{M-M} = −0.15 cm^{-1}) was needed to fully fit the data at low temperatures using the molecular field approximation. The ESR spectrum supported this conclusion. The reason for the lack of any strong interactions was postulated to be due to mismatched orbital energies and symmetries between the Ru_2 dimers and the ligand.

Similar weak antiferromagnetic interactions were also seen in the dicyanamido and tricyanomethenido end-to-end bridged chain species, $[Ru_2(\mu\text{-}O_2CCH_3)_4(\mu\text{-L})]_\infty$ (L = $N(CN)_2^-$ and $C(CN)_3^-$), synthesized by Dunbar and coworkers [29]. For the former J_{M-M} = −0.33 cm^{-1} (D = 63.3 cm^{-1}) and for the latter J_{M-M} = −0.22 cm^{-1} (D = 58.0 cm^{-1}) using the same molecular field approach of Handa. The low values for the dicyanamido derivative were rationalized to be due to weak interactions through its pπ orbitals (these being of the correct symmetry match to interact with the π* orbitals on the Ru_2(II,III) center). When dicyanamide binds in an end-to-end fashion there is reduced electron density on the terminal nitrogens. A similar argument is used for the tricyanomethanide compound with possibly even lower electron density on the bound terminal nitrogens due to the additional "free" cyano group. In addition the rotation angle between the Ru_2 centered π* orbital(s) and the pπ orbital on the terminal nitrogen of the bridge deviate significantly from the optimum 0° in both cases, leading to poorer overlap.

Handa et al. also synthesized two complexes with anthraquinone (aq) as the bridging ligand [30]. One consisted of a "dimer of dimers", $[\{Ru_2(\mu\text{-}O_2CMe_3)_4(H_2O)\}_2(aq)](BF_4)$, with water molecules in the other axial sites. This complex had a large ZFS (D = 70 cm^{-1}) but was deemed to have a very weak antiferromagnetic interaction (similar to the tcnq derivative mentioned above) though no J_{M-M} values were given. The second was a zig-zag chain complex of alternating $[Ru_2(\mu\text{-}O_2CMe_3)_4]^+$ and reduced aq^- units, namely $[Ru_2(\mu\text{-}O_2CMe_3)_4(aq)]_n$, of which a crystal structure was reported but no magnetic data given.

5.3. Metal-complex bridged derivatives

In addition to organic bridging ligands, paramagnetic (and diamagnetic) metal complexes have also been used in linking mixed-valent Ru_2(II,III) centers. Miller and coworkers reported on three compounds with the general stoichiometry $[Ru_2(\mu\text{-}O_2CMe)_4]_3[M^{III}(CN)_6]$ with M = Cr, Fe and Co [31]. No X-ray structure was reported but all three compounds were proposed to assume a network structure consisting of M–C≡N–Ru=Ru–N≡C–M linkages in three dimensions (Fig. 8).

In the case of the compound containing the diamagnetic Co^{III} center the variable temperature magnetic susceptibility data (Fig. 9) could easily be fit using O'Connors model for linked Ru_2(II,III) units (see p. 177 in [1]) yielding essentially no interactions between the centers and a large zero-field splitting of D = 69.4 cm^{-1}. For the Cr^{III} and Fe^{III} derivatives the situation is not as simple. In both cases, a sharp increase in μ_{eff} is seem at low temperatures, at ∼50 K (for Cr^{III}) and ∼8 K (for Fe^{III}) with the former reaching a maximum of 30.9 B.M. at 32 K before it quickly drops to 3.65 B.M. at 2 K, the latter simply increasing to 19.2 B.M. by 2 K.

For both of these cases fitting the data to O'Connor's model exclusively was not sufficient and the additional susceptibility contribution from the paramagnetic bridge center, χ_M, must be taken into account. The typical equation for this

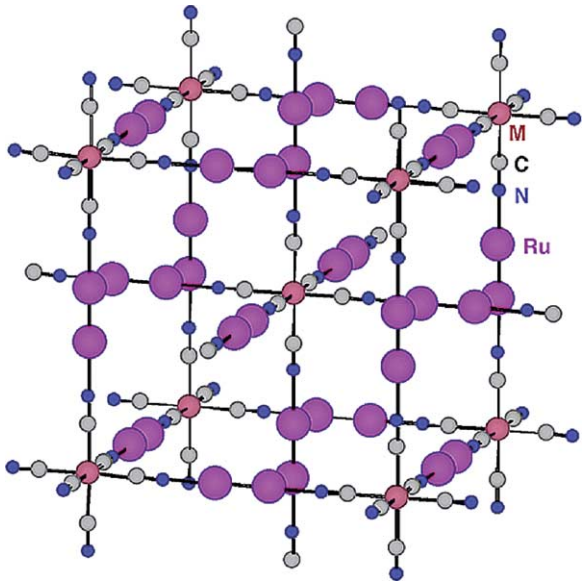

Fig. 8. Proposed 3-D body-centered, interpenetrating network structure for $[Ru_2(\mu\text{-}O_2CMe)_4]_3[M^{III}(CN)_6]$ (M = Cr, Fe, Co); the bridging acetates, rotated by 45° with respect to $[M^{III}(CN)_6]^{3-}$, are not shown for clarity. Reproduced from [31], with permission of the copyright holders.

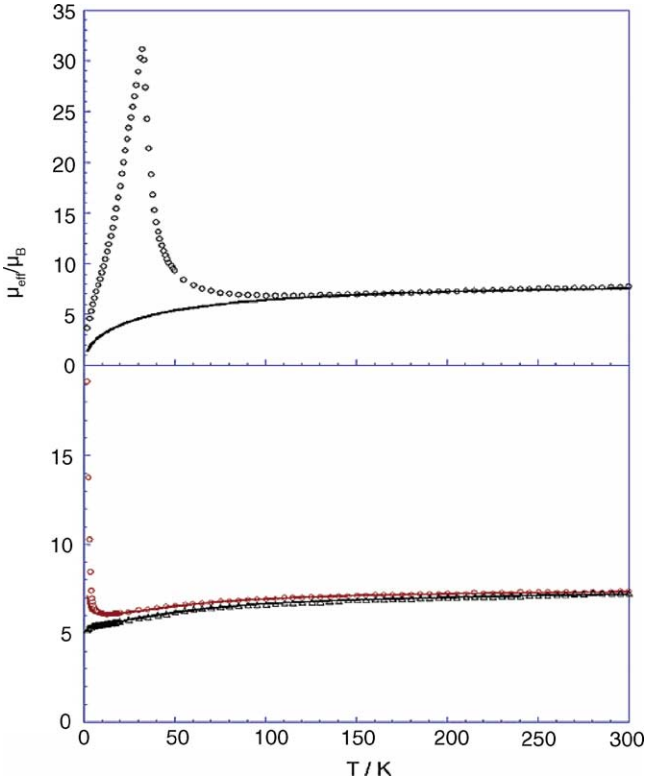

Fig. 9. $\mu_{eff}(T)$ and the fit to the higher temperature data using Eq. (2) (see text) for the M^{III} = Cr (top frame), M^{III} = Fe (top curve in bottom frame) and M^{III} = Co (bottom curve in bottom frame). Reproduced from [31], with permission of the copyright holders.

is given as (1) where the Weiss constant, θ, gives a rough estimate of the magnetic interactions between the paramagnetic species and the overall susceptibility (which now includes the three Ru_2 cores from O'Connor's model, $\chi_{Ru,}$ and the additional bridge metal center, χ_M) is given as χ_{Tot} in Eq. (2). (Note that χ_{Ru} is the same as χ_{av} in reference [1].)

$$\chi_M = \frac{Ng^2\mu^2}{3k_B(T-\theta)}[S(S+1)] \quad (1)$$

$$\chi_{Tot} = 3\chi_{Ru} + \chi_M \quad (2)$$

Using Eq. (2) the fitted data for the Cr^{III} derivative yields $D = 69.4\,cm^{-1}$ and $\theta = -40\,K$ indicating significant antiferromagnetic coupling between the adjacent spin centers. This behaviour is indicative of magnetic ordering and *ferrimagnetic* ordering was confirmed by alternating current susceptibility measurements which yielded a $T_c = 33 \pm 1\,K$. However, saturation magnetization measurements yielded an M_s that was only half the value that would be expected for antiferromagnetic coupling (17,870 emu Oe/mol versus 33,500 emu Oe/mol). This low value was thought to be due to the high D value for the ruthenium dimer. Additional measurements lead to the implication of metamagnetism but more work needed to be done. The Fe^{III} derivative data was fit with $D = 69.4\,cm^{-1}$ and $\theta = 0.7\,K$. The sharp increase at 8 K suggests a transition to long-range ordering as well, but no peak is observed above 2 K suggesting that any ordering occurs below this temperature.

Shortly after the work of Miller appeared, Handa reported on very similar complexes with M = Fe^{III} and Co^{III} of the form $\{[Ru_2(\mu\text{-}O_2CCMe_3)_4]_3(H_2O)M^{III}(CN)_6\}$ [32]. Handa was able to obtain crystal structures of both as tetrahydrates and found them to be isostructural. Contrary to the structural arrangement Miller had proposed for his systems Handa found that the Ru_2 units in his complexes were linked in a 2-D array by the $[M(CN)_6]^{3-}$ bridges into 28-membered $[-M-CN-Ru_2-NC-]_4$ rings. The 2-D network was linked into a 3-D array through hydrogen-bonding between a terminal CN group and the axial water molecule in one of the axial sites on the Ru_2 units. This difference between Miller and Handa's structure is almost certainly due to the nature of the starting reagents. Miller employed $Ru_2(\mu\text{-}O_2CCH_3)_4Cl$ whereas Handa used the di-aqua adduct, $[Ru_2(\mu\text{-}O_2CCMe_3)_4(H_2O)_2](BF_4)$.

Despite the structural differences the magnetic behaviour for the Fe^{III} derivative is similar to that seen by Miller. Handa's Fe^{III} derivative shows an abrupt increase in μ_{eff} at around 20 K, reaching a maximum of 10.34 B.M. at 8 K before decreasing. This indicates ferrimagnetic behaviour and long-range ordering at a slightly higher temperature than observed by Miller. For the Co^{III} complex the data above 10 K was fit to a Curie–Weiss expression with $\theta = -23$ and it was concluded that there *was* antiferromagnetic coupling. Unfortunately, the zero-field splitting was not considered, and a direct comparison with Miller's data (which took D into account and found no interactions) cannot be made.

5.4. Effect of varying the nature of the carboxylate group on the magnetic properties of halide bridged-complexes

The effect of varying the nature of the bridging carboxylate, both in length and in bulk, on the magnetic properties of Ru_2-halide chains has not been extensively investigated. Some studies of Jiménez-Aparicio and coworkers have sought to determine the effect of this change on, in particular, the Ru–Cl–Ru bond angle in complexes of the form $Ru_2(\mu\text{-}O_2CR)_4Cl$ and how this would subsequently effect any antiferromagnetic coupling seen between adjacent Ru_2 dimers [33]. They synthesized two new chain complexes, $\{Ru_2(\mu\text{-}O_2CR)_4Cl\}_n$ with R = –CH=CHCH=CHCH$_3$ and –CH$_2$OMe and the Ru–Cl–Ru angles being 119.43(4)° and 110.11(7)°, respectively (the latter being the most acute Ru–Cl–Ru angle seen in any complex of this type to date). Magnetic measurements were performed on these polymers and contrasted with measurements on three discrete molecular units, $Ru_2(\mu\text{-}O_2CR)_4Cl$ (R = CHMe$_2$, CMe$_3$ and C$_4$H$_4$N) which had been studied previously but only fitted to a simple Curie–Weiss law in the temperature range 70–300 K [34,35]. For the more recently synthesized compounds in [33], it was found that O'Connor's model was insufficient in fitting the data properly at low temperatures, even when corrections for temperature-independent paramagnetism (TIP) and paramagnetic impurities were included. The use of the molecular field approximation, also developed by O'Connor (see p. 179 of [1]), was needed which takes into account both the strong ZFS and the weak intermolecular antiferromagnetism thought to exist in such systems. Using this model, D values ranged from 53.9 to 68.1 cm^{-1}. The antiferromagnetic coupling constants for the discrete units were all very small and ranged form −0.09 to −0.13 cm^{-1}. The two polymers displayed somewhat stronger coupling, despite the acute Ru–Cl–Ru angle, with zJ = −2.84 for R = –CH=CHCH=CHCH$_3$ and zJ = −0.69 for R = –CH$_2$OMe. (It should be noted that the stronger interaction is seen in the chain with the larger Ru–Cl–Ru angle.) The authors argue though (as Cotton et al. had done previously [36]), that due to the Ru–Cl–Ru angle being less than 125° in the chains and the non-negligible zJ values for the discrete units, that the spin-exchange occurs via a *through-space* mechanism (despite the apparent angle correlation mentioned above). It would seem that more data is needed for this argument to be conclusive.

The situation appears clearer when the Ru–Cl–Ru bond angle is closer to 180°. In these cases, strong intrachain antiferromagnetic interactions are usually observed and O'Connor's model cannot be used to fit the data since it does not predict a maximum (T_c) in the χ versus T plot. Cotton's use of an Ising model on such systems [36] is also not entirely satisfactory as it does not take into account the large ZFS inherent in all of these complexes. As a consequence Jiménez-Aparicio and coworkers developed two fitting models to describe systems with strong antiferromagnetic coupling and large ZFS and applied them to the three linear chain complexes, $[Ru_2(\mu\text{-}O_2CR)_4Cl]_n$ where R = –CH$_2$–CH$_3$, –C(Me)=CHEt and –CMePh$_2$, which show T_c values of 35, 32 and 67 K, respectively [37]. One model employs a full-spin Hamiltonian for a linear chain with the magnetic susceptibility calculated using a thermodynamic expression instead of the usual Van Vleck equation and is relatively complex. This model assumes magnetic coupling only between adjacent Ru_2 units with no coupling over longer distances (Scheme 3). The second model is the same in all respects however it uses the Van Vleck formulation with ZFS and antiferromagnetic coupling included to calculate the theoretical magnetic susceptibility. The authors provide a full derivation of both formulations and readers are referred to [37].

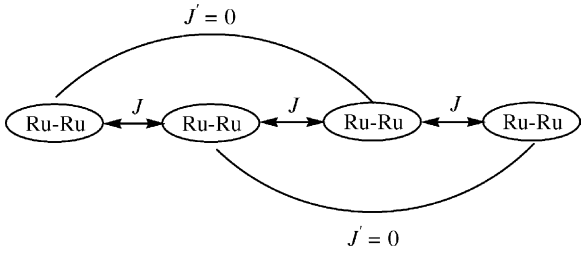

Scheme 3. Magnetic exchange model for linear $[Ru_2(\mu\text{-}O_2CR)_4Cl]_n$ chains.

Both models gave satisfactory fits to the magnetic moment data for all three complexes. The determined values are (with the second model data in parenthesis): D = 46.7 (46.6) cm^{-1}, zJ = −8.05 (−8.02) cm^{-1} for R = –CH$_2$–CH$_3$; D = 48.0 (47.9) cm^{-1}, zJ = −7.46 (−7.43) cm^{-1} for R = –C(Me)=CHEt; and D = 38.1 (37.8) cm^{-1}, zJ = −13.28 (−13.30) cm^{-1} for R = –CMePh$_2$. All of the zJ values are higher than values for non-linear (zig-zag) chain complexes and indicative of relatively strong antiferromagnetism.

More recently additional magnetic measurements were carried out by the same research group on discrete mixed-adduct complexes of stoichiometry $[Ru_2(\mu\text{-}O_2CR)_4X(H_2O)]$ where R = –CH$_2$CH$_2$OPh and X = Cl$^-$ and I$^-$; R = –CMePh$_2$ and X = Cl$^-$, Br$^-$ and I$^-$ [38]. As seen previously all five of these compounds display large ZFS values (D = 50.6–64.7 cm^{-1}) and very small but significant zJ values (−0.07 to −1.33 cm^{-1}) indicative of antiferromagnetic through-space spin-exchange similar to that mentioned for the earlier discrete complexes. A linear-chain complex, $[Ru_2(\mu\text{-}O_2CCH_2CH_2OPh)_4Br]_n$, was also characterized (the first known with a Br$^-$ bridge) and displayed strong antiferromagnetism. Using the models above they were able to fit the data successfully to D = 62.99 cm^{-1} and zJ = −9.08 cm^{-1}. The larger zJ value being characteristic of the polymeric chains with Ru–X–Ru angles of 180°.

When the discrete adducts are heated to drive off the solvated water molecules the anhydrous $[Ru_2(\mu\text{-}O_2CR)_4X]$ species are formed, however, the magnetic data could not be fitted due to a proposed mixture of linear and zig-zag chains (each with its own unique magnetic properties) being formed.

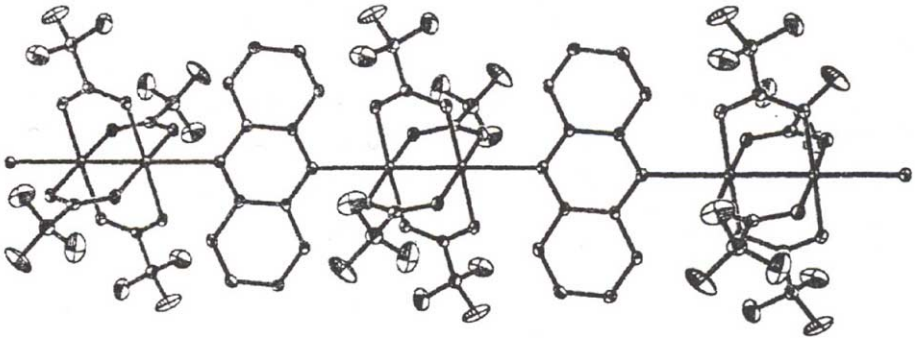

Fig. 10. Structure of the chain compound, $[Ru_2(\mu\text{-}O_2CCF_3)(Phz)]_n$. Reproduced from [39], with permission of the copyright holders.

5.5. Ru_2(II,II) derivatives

While studies on the magnetic behaviour of mixed-valent Ru_2(II,III) based complexes and chains are numerous, very little work has been done on the homovalent, double-bonded, Ru_2(II,II) complexes, in part, due to their air-sensitive nature. The ground-state electronic configuration in this case is thought to be $(\pi^*)^2(\delta^*)^2$ leading to the double bond and an $S = 1$ spin-state. Dunbar and coworkers [39] have recently synthesized the first Ru_2(II,II) containing polymers to be structurally characterized. $[Ru_2(\mu\text{-}O_2CCF_3)_4(phz)]_\infty$ where phz = phenanzine displays relatively linear Ru–Ru–N bond angles however there is some canting away from linearity (15°) by the phananzine units with Ru–N $\cdots$ N angles being about 165° (Fig. 10).

Magnetic measurements revealed a decrease in χT as the temperature is lowered, again, primarily due to the ZFS. The behaviour and fitting process, using the molecular field model, is very similar to that mentioned for the Ru_2(II,III) species and the fitted parameters were found to be $zJ = -3.0\,cm^{-1}$ and $D = 277\,cm^{-1}$. The weaker antiferromagnateic coupling being due to the less than ideal orbital overlap caused by the 15° canting angle. The larger D values are typical for Ru_2(II,II) species.

Handa and coworkers investigated the magnetic properties of the $[Ru_2(\mu\text{-}O_2CCH_3)_4L]_n$ polymers, where L = pyrazine (pyz), 4,4′-bipyridine (4,4′-bpy) and 1,4-diazabicyclo[2.2.2]octane (dabco) [40]. The oxidized, Ru_2(II,III), analogues of these had been investigated earlier by Cukiernik et al. [41] and Aquino and coworkers [42] (these are mentioned in [1]) and found to be weakly coupled antiferromagnetically with zJ values ranging from -0.59 to $-2.3\,cm^{-1}$. Handa's complexes were even more weakly coupled and they concluded that the interdimer interactions were negligibly small compared to the ZFS which was found to be much larger for the Ru_2(II,II) analogues at around 260–290 cm^{-1} (see also Dunbar's work above) versus the Ru_2(II,III) derivatives where the ZFS is on the order of 60 cm^{-1}. Handa also looked at the conductivity properties of all three polymers and found them to be insulators ($\sigma \sim 10^{-10}\,S\,cm^{-1}$). The conductivities could be increased up to values of $\sigma = 10^{-6}\,S\,cm^{-1}$ by doping with the oxidant ferrocenium tetrafluoroborate.

5.6. Theoretical aspects

Numerous magnetic and spectroscopic studies have been performed in order to understand the electronic structures of both the Ru_2(II,III) and Ru_2(II,II) species, however, theoretical calculations that correlate with the experimental results have been few [1]. In addition, the nature of the ground-state for the Ru_2(II,II) complexes ($(\pi^*)^3(\delta^*)^1$ versus $(\pi^*)^2(\delta^*)^2$, with the latter being favoured more recently) has not been entirely resolved. With this in mind Estiú and Cukiernik [43] have performed high level ZINDO/S-MRCI (Zerner intermediate neglect of differential overlap at the self-consistent field multireference configuration interaction) and density functional theory (DFT) calculations and compared them to previous $X\alpha$ calculations of Norman et al. [44] as well as experimental data where possible.

The electronic structure is dependent on the nature of the axial ligands. Axial-ligand free complexes were looked at theoretically because of simplicity. For the Ru_2(II,II) complexes with no axial ligands, $Ru_2(\mu\text{-}O_2CH)_4$, the ZINDO/S-MRCI calculations (Fig. 11) partially agree with the previous work of Norman in that the δ^* orbital is stabilized with respect to the π^*, however the σ^* orbital was also found to be occupied leading to a $(\pi^*)^2(\delta^*)^1(\sigma^*)^1$ quintet state (instead of the triplet $(\pi^*)^2(\delta^*)^2$ which was found to lie 0.024 a.u. higher in energy). Unfortunately there is no experimental data for these isolated cores as even in non-coordinating solvents the dimer units tend to oligomerize. When axial ligands, such as H_2O, are introduced into the theoretical calculations (i.e. $Ru_2(\mu\text{-}O_2CH)_4(H_2O)_2$) a significant change takes place. The σ^* orbital is destabilized and the triplet $(\pi^*)^2(\delta^*)^2$ ground-state is confirmed with the δ^* lying just slightly higher in energy than the π^*. Similar results were obtained with π coordinating ligands such as pyrazine.

The DFT calculations yield a $(\pi^*)^2(\delta^*)^2$ ground-state for all three types of complexes with the σ^* lying higher in energy in all cases. The $(\pi^*)^3(\delta^*)^1$ triplet lies 0.012 au higher in the axial-ligand free species. The discrepancy between the

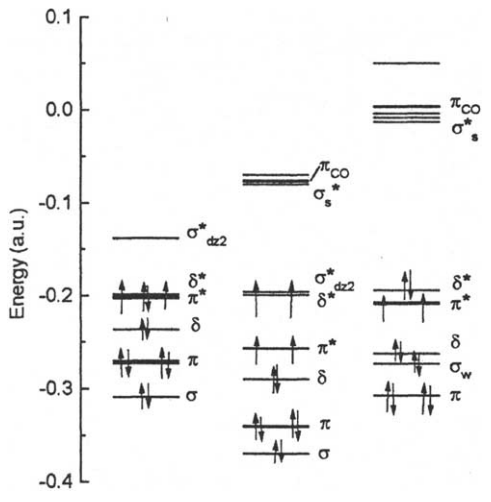

Fig. 11. MO diagrams for divalent $Ru_2(\mu\text{-}O_2CH)_4$, as calculated by *Xα* (left, from [44]) and ZINDO/S-MRCI (middle) as well as for $Ru_2(\mu\text{-}O_2CH)_4(H_2O)_2$ (right) from ZINDO/S-MRCI calculations (energy in a.u.). Reproduced from [43], with permission of the copyright holders.

two methods in the axial-ligand free case is due to the difficulty in modeling such a species as even in non-coordinating solvents the oligomers formed can still be viewed as axially bound entities with oxygen atoms from neighbouring dimers as ligands and no true "naked" species would exist as such. The slight differences in the theoretically predicted MO ordering in the three species allowed the authors to explain the differences seen in the solution and solid electronic and resonance Raman spectra as the axial ligand was varied.

In the case of the Ru_2(II,III) species, the agreement between the electronic ground-state as predicted from the ZINDO calculations (Fig. 12) and Norman's earlier Xα results are quite good. For $[Ru_2(\mu\text{-}O_2CH)_4]^+$ the ground-sate is the quartet $(\pi^*)^2(\delta^*)^1$ as seen by Norman and this also

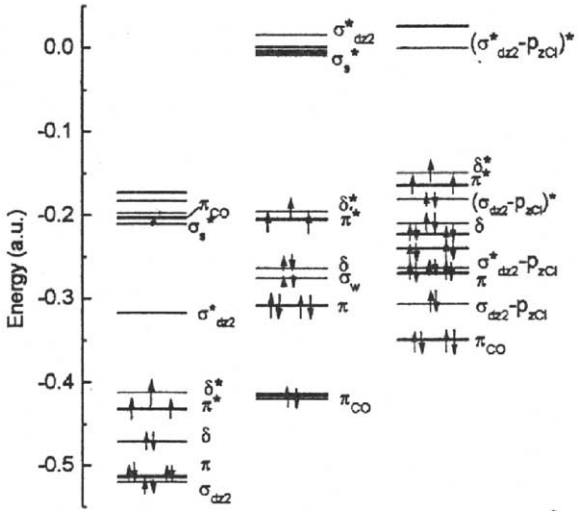

Fig. 12. MO diagrams for mixed-valent $[Ru_2(\mu\text{-}O_2CH)_4]^+$ (left), $[Ru_2(\mu\text{-}O_2CH)_4(H_2O)_2]^+$ (middle), and $[Ru_2(\mu\text{-}O_2CH)_4Cl_2]^-$, (right), from ZINDO/S-MRCI calculations (energy in a.u.). Reproduced from [43], with permission of the copyright holders.

has plenty of experimental support. The π^* and δ^* orbitals lie even closer in energy than in the Ru_2(II,II) case and are near-degenerate. The situation of the HOMO ordering is very similar for the axially bound $[Ru_2(\mu\text{-}O_2CH)_4(H_2O)_2]^+$ and $[Ru_2(\mu\text{-}O_2CH)_4Cl_2]^-$ complexes however both the π^* and δ^* orbitals lie higher in energy, respectively, with respect to the axial-ligand free complex. For the adducts with the π-acid pyrazine or pyridine ligands the HOMO ordering is reversed, due to interaction of the ruthenium π^* orbital with the π system on the N-heterocycle, and the $(\delta^*)^1(\pi^*)^2$ quartet was found to be 0.02 a.u. lower in energy than the $(\delta^*)^1(\pi^*)^2$ doublet in both cases. The DFT calculations for the unligated and Cl^- adducts are in close agreement with the ZINDO calculations.

The theoretical results were used to predict the differences in the electronic band positions seen for the π(RuO) → $\pi^*(Ru_2)$ transition in $[Ru_2(\mu\text{-}O_2CR)_4(L)_2]^+$ at around 450 nm when the nature (particularly donor number) of L was varied. They showed that the wavelengths were lower for L = Cl^- than for L = H_2O, consistent with experimental results. Resonance Raman measurements were also carried out and the $\nu(Ru_2)$ for a series of chloro complexes was measured at around 333 cm^{-1} consistent with the Ru–Ru bond order and the electronic configurations that were proposed. The DFT calculations also predict an increase in overlap of the appropriate magnetic orbitals in complexes of the form $[Ru_2(\mu\text{-}O_2CH)_4\text{–}Cl\text{–}Ru_2(\mu\text{-}O_2CH)_4]^+$ as the Ru–Cl–Ru bond angle approaches 180° and hence a greater degree of antiferromagnetic coupling should be manifested. This has been seen to be the case experimentally (see above).

6. Mesogenic compounds

The last 20 years has seen a very rapid increase in the study of the liquid–crystalline properties of coordination compounds and dimetal tetracarboxylates, $M_2(\mu\text{-}O_2CR_4)$ with M = Cu(II), Rh(II), Mo(II), Cr(II) and Ru(II), have played a large part in this research. Much of the earlier work involving ruthenium complexes focused on the homovalent Ru_2(II,II) species [1] but more recently the mixed-valent Ru_2(II,III) compounds have come under scrutiny and offer a more air-stable and magnetically rich option to the homovalent analogues.

Cukiernik and coworkers thoroughly studied a series of Ru_2(II,III) compounds to see the effect of varying the equatorial carboxylates and the counterions on the mesomorphic properties and concomitant magnetic features [45-48]. They synthesized both linear aliphatic chain complexes of the form $Ru_2(\mu\text{-}O_2C(CH_2)_{n-2}CH_3)_4X$ where X = Cl^- and *n* = 5–9, 12, 16, 18; X = $^-O_2C(CH_2)_{n-2}CH_3$ (pentacarboxylates) and *n* = 6–12, 14, 15, 16; X = dodecyl sulphate (DOS) and *n* = 6, 9, 12, 16, 18; and the branched-chain 3,4- and 3,5-dialkoxybenzoate and 3,4,5-trialkoxybenzoate derivatives of the form $Ru_2(\mu\text{-}x,y,z\text{-}BmOCn)_4Cl$ (where *x*,*y*,*z*-B*m*OC*n* are substituted benzoates, *m* = number of

alkoxy chains on the aromatic ring in positions *x*,*y*,*z* and *n* = number of carbon atoms in each linear alkoxy chain); in particular, Ru_2(μ-3,4-B2OC*n*)$_4$Cl (*n* = 10, 12, 14, 15, 16 and 18), Ru_2(μ-3,5-B2OC*n*)$_4$Cl (*n* = 8, 10, 14 and 18) and Ru_2(μ-3,4,5-B3OC*n*)$_4$Cl (*n* = 1, 8, 10, 12, 14 and 18). In addition, some of these latter complexes were also made with much bulkier anions, i.e. Ru_2(μ-3,4-B2OC*n*)$_4$X with X = 3,4-B2OC*n*$^-$ (pentacarboxylate) or DOS and *n* = 12, 15, 16. Characterization of all of these complexes using IR spectroscopy revealed the diagnostic symmetric and asymmetric carboxyl stretching modes in the 1400–1600 cm^{-1} region. The liquid–crystalline properties were studied using polarized optical microscopy (OM/PL), differential scanning calorimetry (DSC) and powder X-ray diffraction (XRD).

None of the linear chain carboxylates with X = Cl$^-$ displayed a mesophase before their clearing temperature of around 260° which was accompanied by decomposition. It was proposed that the higher homologues form chloride-bridged chains that are perpendicular to each other in the crystal lattice (as opposed to the shorter chain carboxylates such as Ru_2(μ-O_2CCH_3)$_4$Cl and Ru_2(μ-$O_2CCH_2CH_3$)$_4$Cl which display parallel chains) which is not conducive to forming the columnar mesophases, often seen in these types of compounds. Some structural evidence for this does exist with the valerato, Ru_2(μ-$O_2CC_4H_9$)$_4$Cl [46], and butyrato [1] complexes which show two sets of perpendicular cation–anion chains. To overcome this problem and optimize the crystal packing to yield more parallel chains the authors explored three options: (1) the use of a bulky anion with long aliphatic chains, (2) the use of a bulky equatorial carboxylate, and (3) the use of a mix of both large anions and large equatorial carboxylates.

In the first case (bulky anions) all of the linear aliphatic chain pentacarboxylates (those with the equatorial bridge the same as the inter-dimer bridge) showed crystal to columnar hexagonal mesophase transitions (136–167°) that decrease slightly with increasing chain length (Table 3). All of the values are higher than those observed for similar homovalent analogues which display transitions around 100 °C. The measurement of a complex containing a terminally unsaturated fatty acid, undecylenic acid, was also included and it displayed a much lower transition temperature of 119°. Transition enthalpies were found to increase with increasing chain length and are also reported in Table 3. Using XRD the interlamellar distances, *d*, were measured and found to be similar to the homovalent, Ru_2(μ-O_2CR)$_4$, species. The lamellar spacings imply that parallel chains are present. The intercolumnar distances *D* were also reported. The molecular arrangement consists of adjacent polymeric chains axially shifted by half a dimer with interdigitated peripheral fatty acid chains. The repeating distance of 4.4 Å within the chains is close to the 4.3 Å packing distance determined by XRD (Fig. 13) and it was determined that each column of the hexagonal array consists of four entangled molecular chains.

The linear aliphatic chain complexes with X = DOS (as inter-dimer bridge) also show crystal to mesophase transitions around 140 °C and similar enthalpies as the pentacarboxylates (Table 3). Decomposition occurs for all complexes at around 200 °C. The mesophase was characterized as hexagonal columnar but no extensive XRD measurements were undertaken and no *d* or *D* values reported.

Table 3
Temperature (°C) and enthalpy (kJ mol^{-1}) of the crystal-to-mesophase transition for the Ru_2(μ-$O_2C(CH_2)_{n-2}CH_3$)$_5$ and Ru_2(μ-$O_2C(CH_2)_{n-2}CH_3$)$_4$(DOS) series along with interlamellar, *d* (Å), and intercolumnar, *D* (Å), distances in the mesophase (if available)

n	Temperature	Δ*H*	*d*	*D*
Ru_2(μ-$O_2C(CH_2)_{n-2}CH_3$)$_5$				
6	167	21	15.8	–
7	155	26	18.0	–
8	156	33	22.5	–
9	150	45	22.6	–
10	148	48	27.3	30.1
11	152	60	30.0	31.8
12	150	69	32.4	33.9
14	143	84	37.3	36.0
15	136	98	37.7	36.7
16	142	107	42.2	38.7
Ru_2(μ-$O_2C(CH_2)_{n-2}CH_3$)$_5$(DOS)				
6	145	7	–	–
8	121	37	–	–
9	153	36	–	–
12	152	63	–	–
16	140	65	–	–
18	143	118	–	–

The second case (bulky carboxylates and small, chloride, anion) shows varied behaviour depending on the type of substituted benzoate employed (see Table 4). For the 3,4-dialkoxybenzoates (3,4-B2OC*n*) a crystal to a hexagonal columnar mesophase occurs between 129° and 160° for the six compounds studied. While the calculated diameter for the *n* = 15 derivative with fully extended peripheral chains was about 50 Å, the intercolumnar distance, *D*, was found to be about 30 Å which pointed to significant interdigitation

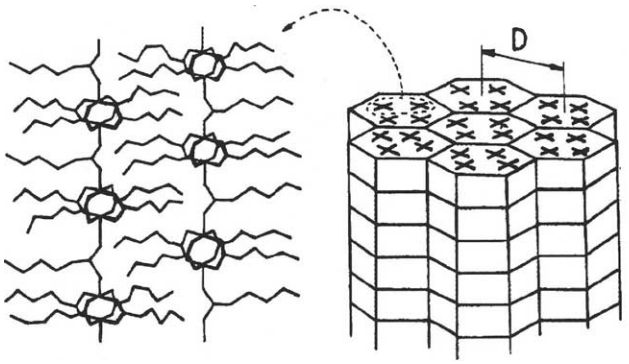

Fig. 13. Schematic representation of the structural model proposed for the thermotropic mesophase of mixed-valent diruthenium pentacarboxylates. Left: two polymeric chains shifted by half a dimer, as supposed to be present in the mesophase of the long-chain mixed-valent diruthenium pentacarboxylates. Right: columnar hexagonal mesophase of these compounds. Each column is built up by four polymeric chains. Adapted from [45], with permission of the copyright holders.

Table 4
Temperature (°C) and enthalpy (kJ mol^{-1}) of the crystal-to-mesophase or mesophase-to-mesophase transition of the $Ru_2(\mu$-*x,y,z*-B*m*OC*n*$)_4$X (X = Cl^-, DOS or *x,y,z*-B*m*OC*n*$^-$) series

x,y,z-B*m*OC*n*[a]	Phase sequence[b]	*T* (°C) (enthalpy, kJ mol^{-1})
X = Cl^-		
3,5-B2OC8	$Col_h \rightarrow Col_h$	43 (4)
3,5-B2OC14	$Col_h \rightarrow Col_h$	67 (88)
3,5-B2OC18	Cr → Col_h	∼40 (135)
3,4-B2OC10	Cr → Col_h	160 (4)
3,4-B2OC12	Cr → Col_h	157 (2.2)
3,4-B2OC14	Cr → Col_h	140 (3)
3,4-B2OC15	Cr → Col_h	150 (2.8)
3,4-B2OC16	Cr → Col_h	157 (4)
3,4-B2OC18	Cr → Col_h	129 (2)
3,4,5-B3OC8	Cr → Col_h	Less than −90
3,4,5-B3OC10	Cr → Col_h	Less than RT[c]
3,4,5-B3OC12	Cr → Col_h	Less than RT[c]
3,4,5-B3OC14	Cr → Col_h	29 (163)
3,4,5-B3OC16	Cr → Col_h	43
3,4,5-B3OC18	Cr → Col_h	58 (273)
X = DOS		
3,4-B2OC12	Cr → Col_h(?)	Less than RT[c]
3,4-B2OC15	Cr → Col_h(?)	Less than RT[c]
3,4-B2OC16	Col_h(?) → LC	41 (220)
X = 3,4-B2OC*n*$^-$		
3,4-B2OC12	Col_h(?) → LC	∼30
3,4-B2OC15	$Col_h \rightarrow$ LC	42 (130)
3,4-B2OC16	Col_h(?) → LC	48 (130)

[a] *x,y,z*-B*m*OC*n* are substituted benzoates, *m* = number of alkoxy chains on the aromatic ring in positions *x*, *y*, *z* and *n* = number of carbon atoms in each linear alkoxy chain.
[b] Cr: crystal phase, Col_h: columnar hexagonal mesophase, LC: indeterminate liquid-crystal phase.
[c] Room temperature.

of the fatty acid chains between adjacent polymers as seen above. The bulkiness of the carboxylates obviously prevented the perpendicular arrangement of chains as implied for the linear aliphatic chain complexes with chloride bridges. For the 3,5-dialkoxybenzoates (3,5-B2C*n*) the two shortest chain analogues (C8 and C14) display room temperature mesomorphism with a transition between two birefringent phases at 43 and 67 °C, respectively and the longer chain derivative (C18) showing a crystal to columnar mesophase transition at 40 °C. The 3,4,5-derivatives (3,4,5-B3C*n*) also show relatively low crystal to mesophase transition temperatures with the C8 analogue manifesting its mesophase lower than the authors were able to measure ($T < -90$ °C).

In the third case (bulky carboxylate *and* bulky anion) both the pentacarboxylate derivatives and the DOS bridged complexes were studied. Both types of compounds appeared to show an ordered columnar hexagonal mesophase (although the only unequivocal proof for this from XRD measurements was for the pentacarboxylate with $n = 15$) at room temperature with, for some, a transition to another indeterminate birefringent phase, which was not fully characterized, before 50°. In the pentacarboxylates the transition temperatures are 30°, 42° and 48° for the $n = 12$, 15 and 16 derivatives respectively and for the DOS bridged analogues a value of 41° was seen for the $n = 16$ derivative (Table 4). All complexes displayed decomposition at ca. 210°. Further study on these important preliminary results is underway but it is clear that there is a strong correlation between molecular structure and liquid-crystallinity in these compounds.

Three of the chloro-bridged alkoxybenzoate derivatives (3,4,5-B3OC14, 3,4-B2OC14 and 3,5-B3OC14) were also investigated for their lytropic behaviour at 40, 70 and 100 °C in dodecane mixtures [49]. While mixing the compounds with 40–60 wt.% of dodecane did not alter the columnar hexagonal mesophase exhibited by the pure compound, there was a marked decrease in the viscosity for all complexes and a depression of the melting point for the 3,4-B2OC14 derivative. At the higher dodecane concentrations and higher temperatures a nematic columnar mesophase was seen prior to the clearing to the isotropic liquid. The formation of the nematic phase was concluded to be due to the swelling of the columns by the incorporation of the solvent. This lead to an increase in the intercolumnar spacings to the point where hexagonal order was lost and a nematic phase formed. At greater than 60% dodecane the mesophase simply dissolved in the solvent.

Variable temperature magnetic susceptibility measurements were performed on some of the above mentioned complexes, both those with and without mesomorphic properties [46]. The molecular field model described earlier was applied to all the data and good fits were obtained for most of the compounds. Not surprisingly, all of the complexes display strong zero-field splittings (*D*) ranging from 60 to 94 cm^{-1}. The *zJ* values for the pentacarboxylates, $Ru_2(\mu\text{-}O_2C(CH_2)_{n-2}CH_3)_5$ where $n = 6$, 8, 9, 12, 14 and 16, indicate antiferromagnetic (AF) exchange and range from −1.7 to −3.2 cm^{-1}. Only one complex with DOS as the counterion/inter-dimer-bridging carboxylate was investigated and $Ru_2(\mu\text{-}O_2C(CH_2)_{14}CH_3)_4$DOS was found to have a very weak AF interaction ($zJ = -0.21$ cm^{-1}). For the Cl^- bridged complexes the linear aliphatic-chain derivatives, $Ru_2(\mu\text{-}O_2C(CH_2)_{n-2}CH_3)_4Cl$, showed similar AF behaviour to those above with $zJ = -4.6$ cm^{-1} for $n = 5$ and $zJ = -0.9$ cm^{-1} for both $n = 8$ and 9, as did the branched chain derivatives, $Ru_2(\mu$-3,4-B2C*n*$)_4Cl$, with $zJ = -2.4$ cm^{-1} for $n = 12$ and $zJ = -3.2$ cm^{-1} for $n = 16$. Assuming the Ru–Cl–Ru bond angle in all of these chloro-bridged long aliphatic-chain complexes is similar to that found for the valerato derivative, $Ru_2(\mu\text{-}O_2CC_4H_9)_4Cl$ ($\angle = 143.2°$), then they lie in an intermediate range (i.e. <180° but >125°) of modest AF interactions.

In all of the above compounds that display mesomorphism, no discontinuity in the magnetic susceptibility curve was observed upon transition to the mesophase indicating that no significant structural, and hence magnetic, changes occur particularly to the binuclear core. For the pentacarboxylate derivatives, this may provide further evidence for each column containing four alternating (–complex–anion–unit) chains, as the interaction within any particular chain should be similar to that in the crystalline phase and any

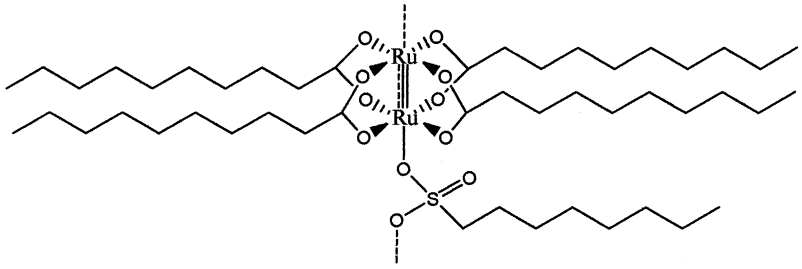

Fig. 14. Schematic drawing of $[Ru_2(\mu\text{-}O_2C(CH_2)_8CH_3)_4][O_3S(CH_2)_7CH_3]$.

interchain interactions would be insignificant because of the bulky peripheral hydrocarbon chains.

A large step forward in interpreting the structural characteristics of mesogenic diruthenium complexes was take when the structure of a decanoate derivative, $[Ru_2(\mu\text{-}O_2C(CH_2)_8CH_3)_4][O_3S(CH_2)_7CH_3]$, was determined (Fig. 14) [50]. This polymeric compound contains an octanesulfonate as its axially bound, bridging, anion and undergoes a transition to a hexagonal columnar mesophase at 185 °C. The Ru_2(II,III) core displays bond lengths and angles typical of the non-mesogenic (shorter-chain) complexes [1]. The four alkyl chains from the carboxylates are oriented toward the periphery of the Ru_2 center in a zig-zag fashion with two chains completely extended and the other two rotated somewhat to align with them. The octyl chain from the interdimer bridging sulfonate anion also aligns itself in an extended conformation parallel to all the carboxylate alkyl chains. The centers of the Ru_2 units are 6.76 Å apart in the polymer chain however the Ru–Ru axes of adjacent units are essentially perpendicular to each other (91.9°). Adjacent polymer chains are separated by a double layer of the non-polar alkyl chains with an interlayer separation of 26.62 Å and no interdigitation between adjacent layers. This is contrary to the conclusions drawn about the bulky long aliphatic-chain derivatives with the chloride bridges, mentioned earlier, where significant interdigitation appeared to be occurring. It is possible that this is due to the small Cl^- versus large octanesulfonate anion bridges, but clearly more structures are needed of the various types of mesogenic complexes to be able to establish a clear structural pattern.

Extensive TGA and DSC measurements were also carried out to determine the thermal decomposition properties of those complexes that displayed mesomorphism [48,51]. The linear aliphatic-chain pentacarboxylates, $(Ru_2(\mu\text{-}O_2C(CH_2)_{n-2}CH_3)_5$ with n = 3–6, 8, 10, 12, 16) were found to decompose in two distinct steps. The first step yielded predominantly the homovalent analogues, $Ru_2(\mu\text{-}O_2CR)_4$, in a one-electron reduction process of the core and concomitant oxidative decarboxylation of the axial anion with homolytic rupture of the Ru–O_{ax} bond (I).

$$Ru_2(\mu\text{-}O_2CR)_5 \rightarrow Ru_2(\mu\text{-}O_2CR)_4 + CO_2 + \text{other products} \quad \text{(I)}$$

This is then followed at higher temperatures by a more dramatic and thermodynamically less favourable reduction to metallic ruthenium which is probably preceded by one or more Ru–O_{eq} bond ruptures and oxidation of the free carboxylates (II).

$$Ru_2(\mu\text{-}O_2CR)_4 \rightarrow 2Ru + xC + yCO_2 + \text{other products} \quad \text{(II)}$$

In all of the cases (n values), the temperature at which the second decomposition occurred remained essentially constant at ≈300 °C however the first decomposition is highly dependent on the chain length. For the complexes that did not display mesomorphism (n = 3–5) the first decomposition temperature dropped from about 300 to about 225 °C. For the higher homologues (n = 6, 8, 10, 12 and 16) which do show an additional crystal to liquid crystal transition in the range of 140–160 °C the first decomposition temperature drops even further from about 215° (n = 6) to about a relatively constant 175 °C for the highest four. It would seem that the appearance of an LC phase provides the added degree of disorder to lower the temperature at which the first reduction occurs. The kinetics of the first decomposition for n = 12 and n = 16 were also studied [48]. In contrast, the linear aliphatic-and branched-chain complexes with Cl^- as the axial bridging ligand displayed only one decomposition process ranging from 300 to 330 °C, corresponding to a process similar to (II). It appears that the stronger reducing power of the axially bound carboxylates (versus the more tightly held and poorer reducing chloride) has a more direct effect on the first reduction process, with concomitant loss of the carboxylate with oxidation.

Except for the undecylenic acid derivative that was briefly mentioned, the introduction of unsaturation into the straight alkyl-chain derivatives of the Ru_2(II,III) derived mesogens has not been looked at but would appear to show promise as the undecylenic acid derivative did show a drop in the transition temperature of 33 °C over its saturated analogue. With this in mind our group decided to investigate this effect further by introducing unsaturation approximately mid-way along the hydrocarbon chain. The polymeric pentacarboxylate, $[Ru_2(\mu\text{-}O_2C(CH_2)_7CH{=}CH(CH_2)_5CH_3)_5]$, which was based on palmitoleic (9-hexadecenoic) acid was synthesized [52]. A crystal to hexagonal columnar mesophase transition was seen at 128 °C which is about 14° lower than the sat-

urated C16 analogue (see Table 3). While this drop in temperature is modest there is a substantial drop in ΔH values, from 107 to 9.6 kJ mol^{-1}, which is mostly due to the presence and the position of the unsaturation. A more interesting feature is that when this material is cooled from 150 °C the mesophase, as seen in the XRD measurements, is maintained down to room temperature for 2–3 days (with a small amount of decomposition) before reverting back to the original crystalline phase. This phenomenon may be due to a supercooling effect which has been seen previously for some homovalent Cu_2(II,II) tetracarboxylate mesogens [53] but is unprecedented for a mixed-valent system.

7. Biological applications

While we have discussed complexes with biologically relevant axial ligands in Section 2.2 the use of these or other Ru_2 tetracarboxylate complexes in drug applications has received limited attention. Only two published studies have appeared in the last 6 years.

The first study involved the synthesis and anti-inflammatory activity of a Ru_2(II,III)-ibuprofenato complex [54]. Ibuprofen or 2-(4-isobutylyphenyl)propionic acid is a carboxylic acid that is an effective non-steroidal analgesic/anti-inflammatory drug (NSAID) and it was investigated to see if binding it to a metal center (or dimetal centers such as Cu_2(II,II) or Ru_2(II,III)) would enhance its anti-inflammatory properties.

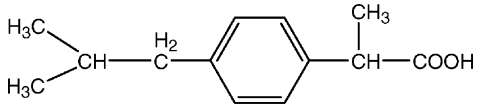

Ibuprofen

$Ru_2(\mu\text{-ibp})_4Cl$ (where ibp = ibuprofenate) was synthesized and characterized by UV–vis and IR spectroscopy, conductance, magnetic susceptibility and thermogravimetric analysis and these were consistent with a polymeric chloride-bridge tetracarboxylate formulation. Oral administration of this complex inhibited the development of carrageenin-induced edema in rats but the inhibitory effects were found to be very similar to that obtained with free ibuprofen, as measured by the volume increase in each rat's hind paw at the time of maximum edema (180 min). However, the metal complex exhibited a marked improvement (a reduction in the lesion index of 50%) in its protective effect with light intensity ulceration over the free ibuprofen. So while the anti-inflammatory properties are unchanged the anti-ulcer properties are significantly improved.

The second study involved the anti-tumor properties of various diruthenium tetracarboxylates. A series of water and alcohol soluble complexes of the type $[Ru_2(\mu\text{-}O_2CR)_4(L)_2](PF_6)$ with L = imidazole, 1-methylimidazole and water when R = CH_3; L = ethanol when R = Fc (ferrocenyl) or Fc-CH=CH–; and of the type $M_3[Ru_2(\mu\text{-}O_2CR)_4(H_2O)_2]\cdot 4H_2O$ with M = Na^+ when R = *m*-$C_6H_4SO_3^-$ and M = K^+ when R = *p*-$C_6H_4SO_3^-$, were tested for cytotoxicity against HeLa and multidrug resistant CoLo 320DM human cancer cells [55]. The latter two sulfonated derivatives (which were highly water-soluble) and the diaquo complex, $[Ru_2(\mu\text{-}O_2CR)_4(H_2O)_2](PF_6)$, showed the most promising results by far. (They were also the most water-soluble of all the complexes studied.) After an incubation period of 7 days the chemosensitivity of the three compounds expressed as IC_{50} (mean drug concentration in μmol dm^{-3} causing 50% cell killing) was 120 for the *meta*-sulfobenzoate derivative, 130 for the *para*-sulfobenzoate derivative and 230 for the diaquo complex against the CoLo 320 DM cancer cell lines and 380, 590 and 950 for the three complexes respectively against HeLa. Particularly satisfying was the observations that in terms of these three complexes, CoLo 320DM, an intrinsically multidrug resistant human colorectal cell line, was 3–4.5 times more prone to drug-induced cell deaths than the human cervix epitheloid cancer cell line (HeLa). This is unusual and opposite to the behaviour of cisplatin.

8. Miscellaneous

The gas-occlusion properties of extended Ru_2(II,III) arrays, incorporating dicarboxylates as equatorial linkers, have recently been studied by Mori and coworkers [56,57]. The use of the dicarboxylates fumarate, *trans–trans*-muconate and terephthalate led to the synthesis of three-dimensional networks based on $Ru_2(O_2C\text{–}CH{=}CH\text{–}CO_2)_2X$, Ru_2(*trans–trans*-$O_2C\text{–}CH{=}CH\text{–}CH{=}CH\text{–}CO_2)_2X$ and $Ru_2(p\text{-}O_2C\text{–}C_6H_4\text{–}CO_2)_2X$ respectively (where X = Cl^- or Br^-). The structure of the terephthalate derivative is shown in Fig. 15. While the dicarboxylates act as linkers in two dimensions the chlorides and bromides provide connectivity in the third. Raman, far-IR and magnetic susceptibility measurements for all three compounds showed similar values to

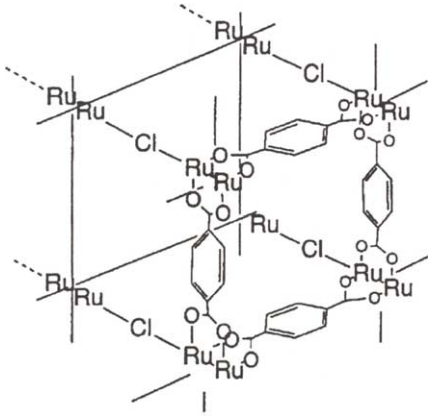

Fig. 15. Three-dimensional structure of $[Ru_2(p\text{-}O_2CC_6H_4CO_2)_2Cl]_n$. Reproduced from [56], with permission of the copyright holders.

those of the parent $Ru_2(\mu\text{-}O_2CCH_3)_4X$ complexes. The interesting feature of all three network structures is their ability to occlude N_2, O_2 and Ar gases below 200 K. The amount of gas occluded increases as the temperature is decreased reaching a maximum (presumably limited by the instrumentation) at liquid nitrogen temperatures. The amounts of N_2 occluded range from 0.7 to 1.3 (mol/mol of Ru atom) for X = Cl^- and 0.6–1.4 for X = Br^-, the amount of O_2 occluded ranged from 1.0 to 1.7 for X = Cl^- and for Ar from 0.8 to 1.4 for X = Cl^- with the higher values being obtained by those structures with the larger cavities, i.e. the muconate and terephthalate derivatives.

This work was extended to the more air-sensitive Ru_2(II,II) core [58] with the synthesis of extended structures incorporating $[Ru_2(p\text{-}O_2C\text{-}C_6H_4\text{-}CO_2)_2]$ and $[Ru_2(p\text{-}O_2C\text{-}C_6H_4\text{-}C_6H_4\text{-}CO_2)_2]$ which formed two-dimensional arrays and $[Ru_2(p\text{-}O_2C\text{-}C_6H_4\text{-}CO_2)_2(dabco)]$ and $[Ru_2(p\text{-}O_2C\text{-}C_6H_4\text{-}C_6H_4\text{-}CO_2)_2(dabco)]$, where dabco = 1,4-diazabicylo[2,2,2]octane, which formed three-dimensional networks. All four of these compounds occlude N_2 gas very well with the maximum amounts ranging from 1.0 to 1.7 mol of gas per mole of ruthenium atoms which is very similar to their Ru_2(II,III) analogues. The pore diameters were measured as well and found to be surprisingly similar for all four compounds at about 8.5 Å however the micropore volumes were larger for axially linked species versus the 2-D compounds and also higher for those with the longer dicarboxylate linkers (biphenyl versus terephthalate).

All four compounds were investigated for their catalytic ability, in particular, the hydrogenation of ethylene at 50 °C. Using 100 mg of complex (pretreated with 120 Torr of H_2 for 1 h) in a closed gas circulation system with a reaction gas consisting of 30 Torr ethylene, 60 Torr H_2 and 1.4 Torr He, 100% conversion to ethane was achieved within 120–324 min. The turnover frequency (TOF) after 5 min was best for the 3-D biphenyl derivative at 6.6×10^{-6} mol of ethane/s atom of Ru and poorest for the 2-D terephthalate derivative at 2.1×10^{-6}. Compared to similar measurements carried out on the mixed-valent $[Ru_2(p\text{-}O_2C\text{-}C_6H_4\text{-}CO_2)_2](BF_4)$ species the TOF values are two orders of magnitude higher here.

The use of the reduced $[Ru_2(\mu\text{-}O_2CR)_4]$ species in alcohol and hexafluorobenzene solutions has shown catalytic activity toward the intermolecular insertion of stabilized diazocompounds (such as diazocoumarin) into the O–H bonds of alcohols and phenols [59]. For example, the reaction of diazocoumarin in methanol in the presence of 3% of $[Ru_2(\mu\text{-}O_2CR)_4]$ gave 3-methoxycoumarin in 95% yield after 2 h of reflux under N_2. This is competitive with, and in some cases better than, the previous catalyst of choice, $[Rh_2(\mu\text{-}O_2CR)_4]$, and significantly cheaper.

A useful and powerful technique for the additional characterization of diruthenium tetracarboxylates is liquid secondary ion mass spectrometry (LSIMS), particularly in the differentiation of polymeric versus non-polymeric $Ru_2(\mu\text{-}O_2CR)_4Cl$-type complexes where X-ray quality crystals may not be readily attainable. Jiménez-Aparicio and coworkers [60] looked at the LSIMS of $Ru_2(\mu\text{-}O_2CCMe_3)_4Cl(H_2O)$, $Ru_2(\mu\text{-}O_2CCHMe_2)_4Cl(thf)$, $Ru_2(\mu\text{-}O_2CR)_4X$ (X = Cl^-, R = CMe_3, $CHMe_2$, $CHEt_2$, CHMePh, Me, C_6H_4-*p*-CMe_3; X = SCN^-, R = CMe_3, $CHEt_2$), and $Ru_2(\mu\text{-}O_2CR)_4X(OPPh_3)$ (X = Cl^-, R = $CHMe_2$, CMe_3; X = SCN^-, R= CMe_3). In most cases, the positive ion of the $Ru_2(\mu\text{-}O_2CR)_4X$ compounds, where X = Cl^- and SCN^-, contains the intact M^+ cations. No molecular peaks were observed for the $Ru_2(\mu\text{-}O_2CR)_4X(OPPh_3)$ complexes (X = Cl^-, SCN^-) but the fragments detected are consistent with the proposed stoichiometry. In addition, MS/MS measurements were made to determine the general fragmentation pathways of the above complexes. The authors also encountered clustering processes, which presumably originated from ion-molecule reactions, giving species such as $[Ru_2(\mu\text{-}O_2CR)_4X\ Ru_2(\mu\text{-}O_2CR)_4]^+$ (X = Cl^- or SCN^-).

The heterogeneous one-electron-transfer rate constant (k_s) for the oxidation of $Ru_2(\mu\text{-}O_2C^tBu)_4$ was measured in benzonitrile by Chisholm and Peters [61]. The formation of the $[Ru_2]^{5+}$ species from the $[Ru_2]^{4+}$ complex involves the removal of an antibonding electron with concomitant increase in the bond-order from 2 to 2.5. For a 1 mM solution of the complex in benzonitrile containing 0.10 M tetrabutylammonium hexafluorophosphate at 25 °C, $E_{1/2}$ = 0.06 V (versus SCE) and $k_s = 2.2(5)\ cm\ s^{-1}$. Measurements were also made on the same complex in the presence of 100 equivalents of pyrazine which led to an increase in the redox potential ($E_{1/2}$ = 0.87 V) and a slight decrease in the rate constant ($k_s = 0.9(6)\ cm\ s^{-1}$). Despite the significantly larger thermodynamic barrier to oxidation the rate of electron-transfer does not appear to be significantly suppressed however the conjugated pyrazine probably does not act as a significant electron conduit either.

Finally, the use of linear assemblies with multiple, redox-active, metal sites have been investigated due to their potential applications in optoelectronics. In the past most such constructs consisted of linked mononuclear metal components. Chen and coworkers [62] utilized the dimeric $[Ru_2(\mu\text{-}O_2CCH_3)_4]^+$ unit and substituted the cyanide containing organometallic complexes, Cp(dppe)FeCN and $Cp(PPh_3)_2RuCN$ (Cp = cyclopentadienyl, dppe = 1,3-bis(diphenylphosphino)ethane), to form the tetranuclear axially bound species $[\{Cp(dppe)FeCN\}_2Ru_2(\mu\text{-}O_2CCH_3)_4](SbF_6)$ and $[\{Cp(PPh_3)_2RuCN\}_2Ru_2(\mu\text{-}O_2CCH_3)_4](SbF_6)$. Axial binding to the Ru_2(II,III) core occurs through the cyanide nitrogen. The CN stretching bands in the IR were found at 2056 and 2063 cm^{-1} for the Fe and Ru derivatives, respectively. This shift to lower frequency from free cyanide was due to a certain degree of π-backbonding from the Ru_2 center. A crystal structure of the Ru derivative was reported (Fig. 16) and confirms the lower CN bond order as the C≡N distance is elongated by about 0.05 Å versus the parent compound. The bond lengths and angles of the $[Ru_2(\mu\text{-}O_2CCH_3)_4]^+$ core are typical of this unit except for a slight elongation of the Ru–Ru bond to 2.2959(10) Å, presumably due to the aforementioned π-backbonding which

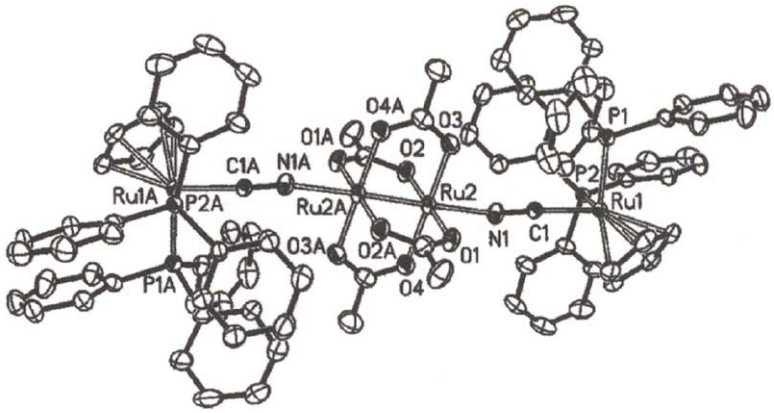

Fig. 16. Structure of the $[\{Cp(PPh_3)_2RuCN\}_2Ru_2(\mu\text{-}O_2CCH_3)_4]^+$ cation. Reproduced from [62], with permission of the copyright holders.

would serve to decrease the amount of bonding electron density. The distance between the two ruthenium atoms on the axially bond $Cp(PPh_3)_2RuCN$ ligands is 12.76 Å.

Cyclic voltammetry measurements were carried out on both complexes and both displayed quasi-reversible redox processes. A cathodic couple corresponding to the reduction of the Ru_2(II,III) core to Ru_2(II,II) was seen at −0.335 V (versus $Fc^{+/0}$) for the Fe derivative and at −0.292 V for the Ru derivative. Anodic couples were seen at +0.658 V corresponding to the oxidation of the Cp(dppe)FeCN in one complex and at +0.986 V for the oxidation of $Cp(PPh_3)_2RuCN$ in the other complex. In both cases, the anodic processes had twice the current intensities of the cathodic processes (which corresponded to one-electron reductions) and it was concluded that in both cases the organometallic axial ligands were oxidized essentially simultaneously, there being no significant electronic interactions over the ∼12.7 Å separation between them. While the mediation of any electronic interaction in the axial direction does not appear promising, this "axial" system should be contrasted with the "equatorial" system discussed in Section 3.2 where there is some interaction (albeit small) between the ferrocenyl units that are separated by 13.5 Å in $[Ru_2(\mu\text{-}O_2CFc)_4(n\text{-}PrOH)_2](PF_6)$.

Acknowledgments

M.A.S.A. gratefully acknowledges NSERC (Canada), the Canadian Foundation for Innovation (CFI) and the University Council for Research (UCR) at St. Francis Xavier University for funding.

References

[1] M.A.S. Aquino, Coord. Chem. Rev. 170 (1998) 141.
[2] A.M. Giroud-Godquin, Coord. Chem. Rev. 178–180 (1998) 1495.
[3] T.M. Buslaeva, S.N. Redkina, O.V. Rudnitskaya, Russ. J. Coord. Chem. 25 (1999) 3.
[4] M.W. Cooke, C.A. Murphy, T.S. Cameron, E.J. Beck, G. Vamvounis, M.A.S. Aquino, Polyhedron 21 (2002) 1235.
[5] G. Vamvounis, J.F. Caplan, T.S. Cameron, K.N. Robertson, M.A.S. Aquino, Inorg. Chim. Acta 304 (2000) 87.
[6] H.J. Gilfoy, K.N. Robertson, T.S. Cameron, M.A.S. Aquino, Inorg. Chim. Acta 331 (2002) 330.
[7] G.G. Briand, M.W. Cooke, T.S. Cameron, H.M. Farrell, T.J. Burchell, M.A.S. Aquino, Inorg. Chem. 40 (2001) 3267.
[8] K.D. Drysdale, E.J. Beck, T.S. Cameron, K.N. Robertson, M.A.S. Aquino, Inorg. Chim. Acta 256 (1997) 243.
[9] M.H. Chisholm, G. Christou, K. Folting, J.C. Huffman, C.A. James, J.A. Samuels, J.L. Weseman, W.H. Woodruff, Inorg. Chem. 35 (1996) 3643.
[10] C. Sudha, A.R. Chakravarty, Ind. J. Chem. A 37 (1998) 1.
[11] H.J. Gilfoy, K.N. Robertson, T.S. Cameron, M.A.S. Aquino, Acta Cryst. E57 (2001) m496.
[12] B.R.A. Bland, H.J. Gilfoy, K.N. Robertson, T.S. Cameron, G. Vamvounis, M.A.S. Aquino, submitted for publication.
[13] F.A. Cotton, J. Lu, A. Yokochi, Inorg. Chim. Acta 275–276 (1998) 447.
[14] M. McCann, F. Humphreys, J. Campbell, A. Carvill, C. Cardin, A. Todd, Polyhedron 16 (1997) 3399.
[15] M.W. Cooke, C.A. Murphy, T.S. Cameron, J.C. Swarts, M.A.S. Aquino, Inorg. Chem. Commun. 3 (2000) 721.
[16] M.W. Cooke, T.S. Cameron, K.N. Robertson, J.C. Swarts, M.A.S. Aquino, Organometallics 21 (2002) 5962.
[17] M.C. Barral, R. Jiménez-Aparicio, J.L. Priego, E.C. Royer, F.A. Urbanos, U. Amador, Inorg. Chim. Acta 279 (1998) 30.
[18] M.C. Barral, R. Jiménez-Aparicio, J.L. Priego, E.C. Royer, F.A. Urbanos, U. Amador, Inorg. Chem. 37 (1998) 1413.
[19] M.C. Barral, R. Jiménez-Aparicio, D. Pérez-Quintanilla, E. Pinilla, J.L. Priego, E.C. Royer, F.A. Urbanos, Polyhedron 18 (1998) 371.
[20] H. Miyasaka, C.S. Campos-Fernández, R. Clérac, K.R. Dunbar, Angew. Chem. Int. Ed. 39 (2000) 3831.
[21] M. Handa, Y. Sayama, M. Mikuriya, R. Nukada, I. Hiromitsu, K. Kasuga, Bull. Chem. Soc. Jpn. 71 (1998) 119.
[22] Y. Sayama, M. Handa, M. Mikuriya, I. Hiromitsu, K. Kasuga, Chem. Lett. (1998) 777.
[23] Y. Sayama, M. Handa, M. Mikuriya, I. Hiromitsu, K. Kasuga, Chem. Lett. (1999) 453.
[24] Y. Sayama, M. Handa, M. Mikuriya, I. Hiromitsu, K. Kasuga, Bull. Chem. Soc. Jpn. 73 (2003) 769.
[25] Y. Sayama, M. Handa, M. Mikuriya, I. Hiromitsu, K. Kasuga, Bull. Chem. Soc. Jpn. 73 (2000) 2499.
[26] Y. Sayama, M. Handa, M. Mikuriya, I. Hiromitsu, K. Kasuga, Bull. Chem. Soc. Jpn. 74 (2001) 2129.
[27] M. Handa, Y. Suyama, M. Mikuriya, R. Nukada, I. Hiromitsu, K. Kasuga, Bull Chem. Soc. Jpn. 68 (1995) 1647.
[28] M. Handa, D. Yoshioka, Y. Suyama, K. Shiomi, M. Mikuriya, I. Hiromitsu, K. Kasuga, Chem. Lett. (1999) 1033.

[29] H. Miyasaka, R. Clérac, C.S. Campos-Fernández, K.R. Dunbar, Inorg. Chem. 40 (2001) 1663.
[30] D. Yoshioka, M. Handa, H. Azuma, M. Mikuriya, I. Hiromitsu, K. Kasuga, Mol. Cryst. Liq. Cryst. 342 (2000) 133.
[31] Y. Liao, W.W. Shum, J.S. Miller, J. Am. Chem. Soc. 124 (2002) 9336.
[32] D. Yoshioka, M. Mikuriya, M. Handa, Chem. Lett. (2002) 1044.
[33] M.C. Barral, R. Jiménez-Aparicio, D. Pérez-Quintanilla, J.L. Priego, E.C. Royer, M.R. Torres, F.A. Urbanos, Inorg. Chem. 39 (2000) 65.
[34] M.C. Barral, R. Jiménez-Aparicio, E.C. Royer, C. Ruiz-Valero, M.J. Saucedo, F.A. Urbanos, Inorg. Chem. 33 (1994) 2692.
[35] M.C. Barral, R. Jiménez-Aparicio, J.L. Priego, E.C. Royer, M.J. Saucedo, F.A. Urbanos, U. Amador, J. Chem. Soc. Dalton Trans. (1995) 2183.
[36] F.A. Cotton, Y. Kim, T. Ren, Polyhedron 12 (1993) 607.
[37] R. Jiménez-Aparicio, F.A. Urbanos, J.M. Arrieta, Inorg. Chem. 40 (2001) 613.
[38] M.C. Barral, R. González-Prieto, R. Jiménez-Aparicio, J.L. Priego, M.R. Torres, F.A. Urbanos, Eur. J. Inorg. Chem. (2003) 2339.
[39] H. Miyasaka, R. Clérac, C.S. Campos-Fernández, K.R. Dunbar, J. Chem. Soc. Dalton Trans. (2001) 858.
[40] M. Handa, D. Yoshioka, M. Mikuriya, I. Hiromitsu, K. Kasuga, Mol. Cryst. Liq. Cryst. 376 (2002) 257.
[41] F.D. Cukiernik, A.-M. Giroud-Godquin, P. Maldivi, J.-C. Marchon, Inorg. Chim. Acta 215 (1994) 203.
[42] E.J. Beck, K.D. Drysdale, L.K. Thompson, L. Li, C.A. Murphy, M.A.S. Aquino, Inorg. Chim. Acta 279 (1998) 121.
[43] G. Estiú, F.D. Cukiernik, P. Maldivi, O. Poizat, Inorg. Chem. 38 (1999) 3030.
[44] J.G. Norman, G.E. Renzoni, D.A. Case, J. Am. Chem. Soc. 101 (1979) 5256.
[45] F.D. Cukiernik, M. Ibn-Elhaj, Z.D. Chaia, J.-C. Marchon, A.-M. Giroud-Godquin, D. Guiilon, A. Skoulios, P. Maldivi, Chem. Mater. 10 (1998) 83.
[46] F.D. Cukiernik, D. Luneau, J.-C. Marchon, P. Maldivi, Inorg. Chem. 37 (1998) 3698.
[47] Z. Chaia, B. Heinrich, F.D. Cukiernik, D. Guillon, Mol. Cryst. Liq. Cryst. 330 (1999) 213.
[48] M. Rusjan, E.E. Sileo, F.D. Cukiernik, Solid State Ionics 159 (2003) 389.
[49] M. Rusjan, B. Donnio, B. Heinrich, F.D. Cukiernik, D. Guillon, Langmuir 18 (2002) 100116.
[50] A. Zelcer, Z.D. Chaia, F.D. Cukiernik, E.C. Castellano, O.E. Piro, Acta Cryst. C58 (2002) m144.
[51] M. Rusjan, E.E. Sileo, F.D. Cukiernik, Solid State Ionics 124 (1999) 143.
[52] J.F. Caplan, C.A. Murphy, S. Swansburg, R.P. Lemieux, T.S. Cameron, M.A.S. Aquino, Can. J. Chem. 76 (1998) 1520.
[53] G.S. Attard, P.R. Cullum, Liq. Cryst. 8 (1990) 299.
[54] A. Andrade, S.F. Namora, R.G. Woisky, G. Weizel, R. Najjar, J.A.A. Sertié, D. de Oliveira Silva, J. Inorg. Biochem. 81 (2000) 23.
[55] C.E.J. van Rensburg, E. Kreft, J.C. Swarts, S.R. Dalrymple, D.M. MacDonald, M.W. Cooke, M.A.S. Aquino, Anticancer Res. 22 (2002) 889.
[56] S. Takamizawa, K. Yamaguchi, W. Mori, Inorg. Chem. Commun. 1 (1998) 177.
[57] S. Takamizawa, T. Ohmura, Y. Yamaguchi, W. Mori, Mol. Cryst. Liq. Cryst. 342 (2000) 199.
[58] T. Ohmura, W. Mori, H. Hiraga, M. Ono, Y. Nishimoto, Chem. Lett. 32 (2003) 468.
[59] S. Cenini, G. Cravotto, G.B. Giovenzana, G. Palmisano, A. Penoni, S. Tollari, Tetrahedron Lett. 43 (2002) 3637.
[60] M.C. Barral, R. Jiménez-Aparicio, J.L. Priego, E.C. Royer, F.A. Urbanos, Inorg. Chim. Acta 277 (1998) 76.
[61] M.H. Chisholm, K.C. Glasgow, L.J. Klein, A.M. Macintosh, D.G. Peters, Inorg. Chem. 39 (2000) 4354.
[62] L.-Y. Zhang, J.-L. Chen, L.-X. Shi, Z.-N. Chen, Organometallics 21 (2002) 5919.